Viscous Irrotational Theories and the Force on an Expanding Bubble: A Cell-Model Analysis

Juan C. Padrino[†] and Daniel D. Joseph*[,†,‡]

Department of Aerospace Engineering and Mechanics, University of Minnesota, Minneapolis, Minnesota 55455, and Department of Mechanical and Aerospace Engineering, University of California, Irvine, California 92697

The dynamics of a bounded viscous incompressible fluid surrounding a spherical bubble in rectilinear motion simultaneously experiencing volume changes is examined by means of two viscous irrotational theories, namely, viscous potential flow and the dissipation method. The forces that the liquid produces on the bubble and on the outer spherical boundary of the liquid are determined from these two approaches at the instant when the bubble is concentric with the outer surface. Viscous potential flow involves surface integration of the irrotational normal stress; the dissipation method stems from the mechanical energy balance, including the dissipation integral, evaluated in potential flow. In the inner boundary, zero tangential stress is enforced. Two choices for the tangential stress condition on the outer boundary are considered: zero tangential stress or irrotational tangential stress. In a sense, this is an extension to include viscous effects of the inviscid analysis by Sherwood [*Int. J. Multiphase Flow*, **1999**, *25*, 705]. The potential flow that follows from Sherwood's work is used in the derived formulas to compute the drag. To the added-mass forces associated with the bubble acceleration and rate of change of the bubble radius determined by Sherwood, a viscous contribution is added here that is dependent on the instantaneous bubble velocity and the inner and outer instantaneous radii of the bubble-liquid cell. When the outer radius is taken to infinity, the expressions for the drag yield results given in the literature. If the inner and outer radii are held fixed, results from the cell model may be used to approximate the drag on a bubble moving in a bubbly suspension with the same volume fraction as the cell. The analysis yields two results for the viscous drag on the bubble, contingent on the boundary condition applied on the outer sphere. These formulas have been presented in the literature, although regarded as contradictories. By emphasizing the role of the tangential stress on the outer boundary, it is shown that both results are valid, because they are dependent on the choice of the outer dynamic boundary condition. These results agree to first order in the volume fraction. The terminal rise velocity of a bubble swarm is derived using the drag from the viscous irrotational theories. Results for the drag coefficient and bubble rise velocity are compared with other theoretical results, as well as data from numerical simulations and experiments, with emphasis in the regime of high Reynolds and low Weber numbers.

1. Introduction

Suspensions of bubbles rising in a liquid in the regime of high Reynolds and low Weber numbers exhibit bubbles that are spherical or almost spherical. Here, these groups are defined in the usual way: the former is defined as $Re \equiv 2Ua/\nu$ and the latter is defined as $We \equiv 2\rho U^2 a/\sigma$ (where U is the bubble velocity, a the bubble radius, ρ the density of the liquid, ν the kinematic viscosity of the liquid, and σ the interfacial tension). Generally, for very high Reynolds numbers (for example, $O(1000)$, from ref 1), the Weber number is likely greater than unity and the bubble shows important deviations from the spherical shape. Experimentally, the dual limit of high Reynolds and low Weber numbers have been realized with $Re = O(100)$ and $We = O(1)$, respectively.[2] For instance, bubbles with a diameter in the order of 1 mm rising in water satisfy the dual condition of high Re and low We.[2,3] Moreover, in this regime, with a clean liquid—that is, free of impurities and surfactants—vorticity effects are confined to a thin boundary layer on the bubble surface and to a wake in a minute neighborhood of the bubble rear end.[1] Therefore, liquid motion in the bulk can be considered to be irrotational. Because of these features, bubbly suspensions in this regime are particularly suited for analysis. Further simplification is attained by considering bubbles of the same diameter, that is, a monodispersed suspension. In practice, small variation about the mean bubble diameter may be achieved by preventing coalescence with the addition of certain chemicals to the mixture in such low concentration that the gas/liquid interface does not behave as the boundary of a rigid particle, in which case a recirculation zone would appear at the rear side of the bubble, thereby breaking down the irrotational hypothesis.[2,4]

For bubbles rising under the action of gravity, the problem also has been described, besides the Reynolds number, by the Eötvös number, which is a characteristic of the bubb le size, and the Morton number, which is a group that involves physical properties with no bubble-size-dependent quantities.[5] Small Eötvös values are associated with almost-spherical bubbles, whereas larger Eötvös values indicate highly distorted bubbles. The Weber number can be recovered by combining those three dimensionless groups. Instead of the Morton number, the Archimedes number may be used.[6]

In modeling bubbly suspensions in the regime of low We and high Re, viscous drag is usually computed from the liquid potential flow solution exploiting the fact that rotational (viscous) deviations from irrotational motion are confined to thin regions adjacent to the bubbles. In this regard, the dissipation method, based on the mechanical energy balance,

* To whom correspondence should be addressed. Tel.: 612-625-0309. Fax: 612-626-1558. E-mail address: joseph@aem.umn.edu.
[†] Department of Aerospace Engineering and Mechanics, University of Minnesota.
[‡] Department of Mechanical and Aerospace Engineering, University of California.

10.1021/ie800251j CCC: $40.75
Published on Web 12/12/2008

has been a commonly used approach. A boundary layer on a clean bubble interface conforms to the zero-shear-stress boundary condition, because of the large viscosity of the liquid compared to the small viscosity of the gas, rather than to the nonslip constraint enforced on a solid particle. This boundary layer remains attached almost over the entire bubble interface, as separation occurs only around the rear end. Since vorticity is contained in these narrow regions, it is assumed that the rate of viscous dissipation is given entirely by the irrotational motion.[7]

For a sphere translating in rectilinear motion with constant speed within an infinite liquid, the dissipation approximation seems to have been applied first by Bateman in 1931 (see the reported work of Dryden, Murnaghan, and Bateman[8]), who obtained a drag of $12\pi a\mu U$, where μ is the liquid dynamic viscosity. Later, Ackeret[9] repeated this dissipation calculation. For a bubble in rectilinear motion, Levich[10] applied the dissipation method and attained the result given above. This drag is close to the measured value for Reynolds numbers above 20.[11] Note that for a rigid sphere, with the no-slip condition enforced at its surface, or a spherical bubble of constant volume, for which the tangential component of the traction vanishes at the interface, the dissipation calculation based on potential flow gives rise the same drag.[11] Moore[12] found the drag $12\pi a\mu U$, which, in dimensionless form, is written as $48/Re$, by computing the momentum deficit. In addition, he determined the structure of the boundary-layer flow and used this information to improve upon the Re^{-1} result by adding a $Re^{-3/2}$ contribution from the dissipation in the boundary layer and wake. Kang and Leal[13] and, recently, Joseph and Wang[14] used different methods to add a viscous correction to the normal stress and obtained $48/Re$. Note that Moore[15] computed a viscous drag by direct integration of the irrotational normal stress around the bubble, thereby enforcing the zero shear stress at the interface. He found the drag to be $8\pi a\mu U$, which fell short of the dissipation result. Evidently, this discrepancy is resolved by adding a viscous correction to the irrotational normal stress.[12−14] Tam[16] extended Moore's[12] analysis to the case of a translating bubble undergoing acceleration and found the same form of the viscous drag. The approach of potential flow with viscous normal stresses at a gas/liquid interface was applied by Miksis, Vanden-Broeck, and Keller[17] to compute numerically the shape of a rising bubble using a boundary-integral formulation.

The effect of a varying bubble radius on the force experienced by a bubble translating in an unbounded liquid has been the subject of several works. Magnaudet and Legendre[18] examined this case by means of a frame transformation under which the bubble radius becomes fixed while conserving dynamic similarity. The total force on the bubble is presented for both the inertia-dominated flow and the creeping flow limits. Ohl, Tijink, and Prosperetti[19] conducted experimental investigations of this bubble motion, whereas Yang, Prosperetti, and Takagi[20] performed numerical simulations. Both works included simplified dynamic models accounting for the forces acting on a bubble that compare favorably with the experimental and numerical data. Takemura and Magnaudet[21] studied experimentally the history force on a shrinking bubble rising at finite Reynolds number. Recently, Léger and Askovic[22] performed the modeling of the boundary layers outside and within a slowly deforming spherical bubble in rectilinear motion. Comprehensive reviews on the advances in the understanding of single bubble dynamics have been given by Magnaudet and Eames[23] and Kulkarni and Joshi.[24]

Dynamic simulations of the motion of a set of N bubbles moving in a liquid at rest at infinity have been examined in several papers (for example, Voinov and Golovin,[25] Gavrilyuk and Teshukov,[26] and Ilinsky, Hamilton, and Zabolotskaya[27]). Smereka[28] studied the motion of a set of bubbles in a box in a periodic assembly, so that the entire space is filled with an array of boxes. Wang and Smereka[29] took the continuum limit of the equations of motion for a finite set of bubbles in an unbounded liquid to obtain effective equations in terms of the void fraction. In these works, potential flow is assumed for the liquid motion and viscous effects are given by the dissipation method. Sangani and Didwania[3] and Kushch et al.[30] performed dynamic simulations with the viscous drag determined from a leading order viscous correction to the irrotational pressure computed from the analysis of the boundary layer flow around the bubbles. The former also estimated the viscous drag on the bubbles with the gradient of the rate of energy dissipation in potential flow. The latter considered arrays of ellipsoids to account for bubble shape deformation such that flows with finite We values may be simulated. On the other hand, averaged equations for bubbly flows derived from first principles have been presented by Sangani[31] and Spelt and Sangani,[32] considering the irrotational motion of a viscous fluid, and in the work of Zhang and Prosperetti[33] for an inviscid fluid. Recently, the buoyant rise of a set of almost-spherical bubbles as well as deformable ones at a Reynolds number of $O(100)$ in a periodic box has been studied through direct numerical simulations of the incompressible Navier−Stokes equations by Esmaeeli and Tryggvason[6] with a front-tracking/finite-volume method. Earlier, these authors[34,35] applied a similar method to study almost-spherical bubbles at $Re = O(1)$ and $Re \approx 20$. Using the same technique, Bunner and Tryggvason[36,37] considered a much larger number of bubbles for the latter Reynolds-number regime. By placing a single bubble in a periodic box, a regular array of bubbles of the same size was simulated by Sankaranarayanan et al.[5] and Yin et al.,[38] using the lattice Boltzmann method for the intermediate-Reynolds-number regime, i.e., $O(10)$. In this regime, the wake effects in the bubble-liquid dynamics cannot be neglected. Careful experiments and detailed measurements have been conducted by Zenit et al.[2] to study bubbly suspensions for small We values and large Re values and by Martinez-Mercado et al.[39] for intermediate and high Reynolds numbers (in the range of $Re = 10-500$).

Effective properties of particulate flows including hydrodynamic transport coefficients have been modeled by means of effective-medium theories. According to these approximate theories, the conditionally averaged field satisfies the suspending fluid equations within a suitably sized exclusion region that encloses a reference particle or bubble and the unconditionally averaged fields in the effective medium occupying the remainder of the space.[40] The method does not bear the ambiguity of the choice of proper constraints at the interface between the effective medium and the exclusion region. Kushch et al.[30] determined the added mass and viscous drag coefficients for a suspension of oblate spheroidal bubbles using an effective medium theory showing remarkable agreement with dynamic simulations. Detailed descriptions of the effective medium theory applied in various contexts can be found elsewhere.[41−44]

A simplified approach to examine the hydrodynamics of a suspension of bubbles moving in a liquid for small or moderate gas volume fraction is obtained through the so-called "cell-model" representation. For almost-spherical bubbles, the bubbly liquid is assumed to be composed of identical unit spherical cells. Each cell consists of a spherical bubble surrounded by a

liquid bounded by an outer spherical envelope concentric with the bubble. The outer sphere radius is such that the cell void fraction is identical to the void fraction of the bubbly liquid.[45] The underlying hypothesis is that the dynamics within the reference cell is representative of the dynamics in the entire bubbly suspension. The choice of the outer boundary condition in the cell model has been subject of debate (see Chhabra[46] and references therein). Happel and Brenner[45] have argued that each cell should be a unit independent of the remainder of the assemblage, so no energy exchange occurs with its surroundings. They thus consider that a frictionless outer boundary is adequate. Other boundary conditions, however, have been applied in the literature. For particulate flows in the limit of creeping motion, Cunningham[47] applied the cell model with nonslip conditions on the inner and outer spherical boundaries. Happel[48] considered the same problem, although imposing a zero-tangential-stress constraint on the outer envelope. Kuwabara[49] applied a zero-vorticity boundary condition on the outer sphere and computed the drag from the dissipation integral evaluated in Stokes' flow. However, in his formulation, as noted by El-Kaissy and Homsy,[50] the term accounting for the work of the tangential stress on the outer envelope is missing. The zero-vorticity constraint implies that mechanical energy is transferred between the reference cell and the remainder of the domain. For higher *Re* values, Marrucci[51] used the cell model to predict the drag on the bubble, evaluating the dissipation integral from the potential flow solution in the cell. Recently, Kendoush[52] revisited Marrucci's analysis, obtaining a different drag. We shall review this discrepancy in section 3. Leclair and Hamielec[53] presented the numerical solution of the Navier−Stokes equations for the liquid motion within a unit cell with zero shear stress on the bubble surface and zero vorticity on the outer sphere. They computed the drag on the bubble with the numerical flow field. Reasonably good agreement with the experimental data was reported. A similar numerical analysis was performed by Manjunath et al.[54] enforcing, in contrast, a zero-tangential-stress condition on the outer boundary. Chhabra[46] also presented numerical results for a viscous liquid in a cell model enclosing a bubble to elucidate the effect on the drag of the choice of either zero tangential stress (free surface) or zero vorticity on the outer boundary. He concluded that the viscous force shows a stronger dependence on the void fraction in the zero-vorticity model than in the free-surface model. All these works have considered a cell enclosing a bubble of constant volume. More recently, Sherwood[55] modeled the dynamics of a translating spherical bubble with a time-dependent radius surrounded by an inviscid imcompressible fluid bounded externally by a spherical surface. He presented expressions for the force on the bubble and on the outer envelope.

After surveying the literature on the cell model, we are left with the impression that the implementation of the dissipation method lacks a systematic approach to deriving expressions for the forces starting from the mechanical energy equation with emphasis in the role of the cell boundary conditions from dynamics (stresses). The objective of this paper is to extend Sherwood's[55] analysis to include viscous effects, using purely irrotational theories, namely, viscous potential flow and the dissipation approximation. The former approach computes the force on a given direction by direct integration of the irrotational normal stress over the boundary, whereas the latter predicts the drag from the mechanical energy balance evaluated in potential flow, so that the viscous effects arise from the rate of energy dissipation. First, working formulas for the drag are developed by applying these theories to the system defined by a spherical bubble with its center moving in a rectilinear path and undergoing volume changes within a bounded liquid domain with a deforming outer boundary. The shape evolution of the inner and outer boundaries is assumed to be known, such that the incompressibility constraint is satisfied. Two different conditions for the tangential stress on the outer boundary are considered, namely, a zero-tangential-stress condition (i.e., free surface) and an irrotational-tangential-stress condition. In the inner boundary (i.e., bubble surface), zero tangential stress is enforced. This is the same as having two boundary-value problems. The dissipation method gives rise to different expressions for the force on the bubble on a given direction, depending on the tangential stress condition applied on the outer boundary of the reference cell. Viscous potential flow, on the other hand, gives the same bubble drag, independent of the choice of the outer boundary condition. Next, the flow field is obtained from Sherwood's potential analysis. This potential flow is then entered in the machinery previously derived to compute the forces on the spherical bubble and on the spherical outer envelope at the instant when both are concentric. This is the same geometric condition for which Sherwood computed the forces. The expressions for the drag on the bubble show the added-mass contribution given by the acceleration of the bubble translational motion and the rate of change of the bubble radius, already given in Sherwood's inviscid analysis, plus a viscous drag, depending on the instantaneous values of the velocity and inner and outer radii. When neither the inner nor the outer radius changes with time, the formulas for the drag are rewritten in terms of the cell void fraction. According to the cell model, these expressions can be used as an approximation for the drag on a typical bubble moving in a swarm of bubbles with the same average void fraction. These results for the viscous drag from the dissipation method have been given in the literature;[51,52] however, the role of the dynamic boundary conditions, in particular, that of the tangential stress on the outer boundary, is not evident there. Because each of these two expressions for the drag corresponds to a different choice of the outer boundary condition for the stress, these results do not contradict each other; neither is one of them in error, as has been argued in the literature.[52] Results indicate that the drag from the model with an irrotational tangential stress on the outer boundary shows a stronger dependence on the void fraction than the drag from a free-surface cell model. Both results for the bubble drag from the dissipation method, however, match to first order in the void fraction. Using the formulas for the drag, expressions for the terminal rise velocity for a bubble swarm in dimensionless form are obtained. Finally, predictions from these analyses are compared with results from other theoretical approaches, numerical simulations, and experiments.

2. Formulas for the Force on an Expanding Bubble within a Bounded Liquid from Viscous Irrotational Theories

We present an analysis that gives rise to the formulas for the force acting on a spherical compressible bubble along its direction of motion within a liquid confined by a spherical surface. Two types of purely irrotational analysis are conducted, namely, viscous potential flow and the dissipation method.

2.1. Problem Formulation. Consider a spherical bubble B moving within a viscous incompressible Newtonian fluid occupying the volume V in three dimensions. Let S_1 be the

interface shared by the bubble B and the liquid in V and let S_2 be the outer spherical surface bounding V (see Figure 1). Both S_1 and S_2 remain spherical during the entire motion. Suppose the center of the bubble moves on a straight line containing the center of the outer sphere S_2 along the direction e_x (fixed) with velocity U, which may be a function of time. Moreover, suppose the bubble volume can change with time but the bubble does not rotate. The pathline followed by the center of the bubble thus defines the axis of symmetry for this configuration. Let $\mathbf{u}$ be the velocity field in the laboratory (inertial) reference frame. Let $\mathbf{v}$ be the velocity field with respect to a noninertial reference frame whose origin moves with velocity $U\mathbf{e}_x$ relative to the laboratory frame, but it is not allowed to rotate. Velocities $\mathbf{u}$ and $\mathbf{v}$ are then related by

$$\mathbf{u} = U\mathbf{e}_x + \mathbf{v} \tag{2.1}$$

The fluid dynamics within the bubble does not enter the analysis. Suppose the following boundary conditions are given:

On S_1:

$$\mathbf{n}_1\cdot\mathbf{v} = \hat{q}_1 \tag{2.2}$$

$$\mathbf{n}_1\cdot\mathbf{T}\cdot\mathbf{t}_1^{(\alpha)} = 0 \qquad (\text{with } \mathbf{t}_1^{(\alpha)}\perp\mathbf{n}_1) \tag{2.3}$$

On S_2:

$$\mathbf{n}_2\cdot\mathbf{u} = q_2 \tag{2.4}$$

$$\mathbf{n}_2\cdot\mathbf{T}\cdot\mathbf{t}_2^{(\alpha)} = \tau_2^{(\alpha)} \qquad (\text{with } \mathbf{t}_2^{(\alpha)}\perp\mathbf{n}_2) \tag{2.5}$$

and $\alpha = 1, 2$. Here, $\mathbf{n}_1$ is the inward unit normal on S_1 to V (i.e., outward to the bubble) and $\mathbf{n}_2$ is the outward unit normal on S_2 to V; $\mathbf{t}_1^{(\alpha)}$ and $\mathbf{t}_2^{(\alpha)}$ are unit vectors. Each triad $\{\mathbf{n}_\beta, \mathbf{t}_\beta^{(1)}, \mathbf{t}_\beta^{(2)}\}$, with $\beta = 1$ or 2, is orthogonal and right-handed. The symbol $\mathbf{T}$ denotes the stress tensor.

Constraint 2.3 is a standard interfacial condition for a bubble, in which case the gas dynamic viscosity is small, in comparison to that of the liquid. We are assuming here that Marangoni stresses, which originate from surface tension gradients, are negligible. This is typical of a clean gas/liquid interface (e.g., free of impurities or surfactants). From expressions 2.1 and 2.2, notice that $q_1 = \mathbf{n}_1\cdot\mathbf{u} = U\mathbf{n}_1\cdot\mathbf{e}_x + \hat{q}_1$ on S_1.

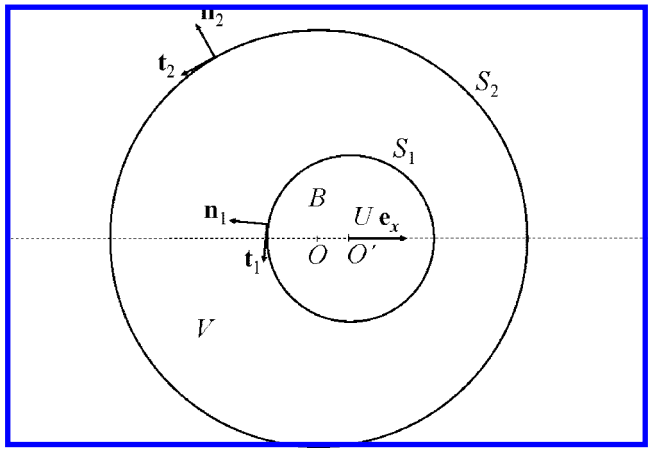

Figure 1. Sketch of a spherical bubble B centered at O' sharing interface S_1 with the incompressible fluid occupying volume V bounded externally by the spherical surface S_2 centered at O. The motion of the bubble B is such that O' moves along the fixed direction $\mathbf{e}_x$ with speed U, and its radius can change with time. The line containing the path of O' also contains O, which is fixed with respect to the laboratory frame. Therefore, this line is the axis of symmetry of the problem. The separation between O and O' is considered to be small. Because of the incompressibility of the fluid in V, changes in the radius of S_2 occur in accordance with changes in the radius of B. The symbol "$\mathbf{n}_1$" denotes the inward unit vector to V on S_1 and the symbol "$\mathbf{n}_2$" denotes the outward unit vector to V on S_2. Unit vectors $\mathbf{t}_1$ and $\mathbf{t}_2$ are orthogonal to $\mathbf{n}_1$ and $\mathbf{n}_2$, respectively.

Two choices for $\tau_2^{(\alpha)}$ in expression 2.5 for the outer boundary are considered in this work, namely, (i) zero tangential stress and (ii) irrotational tangential stress. The latter is established from the potential flow in V, which is fully determined by kinematic boundary conditions, as explained in section 2.2.

Using expressions 2.2 and 2.4, the incompressibility condition and divergence theorem lead to

$$\int_{S_1} \hat{q}_1 \, dA = \int_{S_2} q_2 \, dA \tag{2.6}$$

which establishes a constraint that $\hat{q}_1$ and q_2 must satisfy.

The forces that the fluid in V exerts on S_1 and S_2 in the $\mathbf{e}_x$-direction are

$$D_1 \equiv \int_{S_1} \mathbf{n}_1\cdot\mathbf{T}\cdot\mathbf{e}_x \, dA \tag{2.7}$$

$$D_2 \equiv -\int_{S_2} \mathbf{n}_2\cdot\mathbf{T}\cdot\mathbf{e}_x \, dA \tag{2.8}$$

With the decomposition defined as $\mathbf{e}_x = \mathbf{n}_\beta(\mathbf{n}_\beta\cdot\mathbf{e}_x) + \mathbf{t}_\beta^{(\alpha)}(\mathbf{t}_\beta^{(\alpha)}\cdot\mathbf{e}_x)$, for $\alpha = 1, 2$ and $\beta = 1,2$, with summation over α but not over β, these expressions can be written as

$$D_1 = \int_{S_1} \mathbf{n}_1\cdot\mathbf{T}\cdot\mathbf{n}_1(\mathbf{n}_1\cdot\mathbf{e}_x) \, dA + \int_{S_1} \mathbf{n}_1\cdot\mathbf{T}\cdot\mathbf{t}_1^{(\alpha)}(\mathbf{t}_1^{(\alpha)}\cdot\mathbf{e}_x) \, dA \tag{2.9}$$

$$D_2 = -\int_{S_2} \mathbf{n}_2\cdot\mathbf{T}\cdot\mathbf{n}_2(\mathbf{n}_2\cdot\mathbf{e}_x) \, dA - \int_{S_2} \mathbf{n}_2\cdot\mathbf{T}\cdot\mathbf{t}_2^{(\alpha)}(\mathbf{t}_2^{(\alpha)}\cdot\mathbf{e}_x) \, dA \tag{2.10}$$

Invoking constraints 2.3 and 2.5, we have

$$D_1 = \int_{S_1} \mathbf{n}_1\cdot\mathbf{T}\cdot\mathbf{n}_1(\mathbf{n}_1\cdot\mathbf{e}_x) \, dA \tag{2.11}$$

$$D_2 = -\int_{S_2} \mathbf{n}_2\cdot\mathbf{T}\cdot\mathbf{n}_2(\mathbf{n}_2\cdot\mathbf{e}_x) \, dA - \int_{S_2} \tau_2^{(\alpha)}(\mathbf{t}_2^{(\alpha)}\cdot\mathbf{e}_x) \, dA \tag{2.12}$$

It is assumed, in this analysis,that the geometry of the fluid domain V is known at any time. For the sake of simplicity, we have taken hydrostatics forces (i.e., buoyancy) out of the analysis.

2.2. Viscous Potential Flow. The viscous potential flow approximation of the forces on surfaces S_1 and S_2 is obtained by direct integration of the stress computed for purely irrotational motion. For a free-shear surface, where the actual tangential stress is zero, only the normal stress enters in the viscous potential flow computation, although the irrotational tangential stress is not zero.

For irrotational motion, the velocity field is $\mathbf{u} = \nabla\phi = U\mathbf{e}_x + \mathbf{v}$. For incompressible flow, the potential satisfies

$$\nabla^2\phi = 0 \tag{2.13}$$

with boundary conditions

$$\mathbf{n}_1\cdot\nabla\phi = q_1 = U\mathbf{n}_1\cdot\mathbf{e}_x + \hat{q}_1 \tag{2.14}$$

on S_1, and

$$\mathbf{n}_2\cdot\nabla\phi = q_2 \tag{2.15}$$

on S_2. The irrotational pressure p satisfies the Bernoulli equation:

$$\frac{p}{\rho} + \frac{\partial\phi}{\partial t} + \frac{|\mathbf{u}|^2}{2} = C(t) \tag{2.16}$$

The forces on the boundaries of V are computed according to expressions 2.11 and 2.12 for irrotational motion. Thus, for a Newtonian fluid, the stress tensor is given by

$$T = -p\mathbf{1} + 2\mu\nabla \otimes \nabla\phi \tag{2.17}$$

Hereinafter, for the sake of brevity, we use the symbol $\mathbf{D}$ to refer to the strain-rate tensor in potential flow ($\mathbf{D} \equiv \nabla\otimes\nabla\phi$).

On the free-shear surface S_1 or bubble interface, the force in the $\mathbf{e}_x$-direction is

$$D_1 = \int_{S_1} (-p + \mathbf{n}_1\cdot 2\mu\mathbf{D}\cdot\mathbf{n}_1)\mathbf{n}_1\cdot\mathbf{e}_x \, dA \tag{2.18}$$

The force on the outer free surface S_2 in the $\mathbf{e}_x$-direction is, for zero tangential stress,

$$D_2 = -\int_{S_2} (-p + \mathbf{n}_2\cdot 2\mu\mathbf{D}\cdot\mathbf{n}_2)\mathbf{n}_2\cdot\mathbf{e}_x \, dA \tag{2.19}$$

In the case of an outer boundary subject to a tangential stress given by the potential flow in the interior, that is,

$$\tau_2^{(\alpha)} = \mathbf{n}_2\cdot 2\mu\mathbf{D}\cdot\mathbf{t}_2^{(\alpha)} \tag{2.20}$$

the self-equilibration of irrotational viscous stresses on a closed surface (Appendix B) implies

$$\int_{S_1} \mathbf{n}_1\cdot 2\mu\mathbf{D}\cdot\mathbf{e}_x \, dA = \int_{S_2} \mathbf{n}_2\cdot 2\mu\mathbf{D}\cdot\mathbf{e}_x \, dA = 0 \tag{2.21}$$

Hence,

$$D_2 = -\int_{S_2} (-p)\mathbf{n}_2\cdot\mathbf{e}_x \, dA \tag{2.22}$$

Thus, the force on the outer boundary is obtained solely from the irrotational pressure in this case.

2.3. Dissipation Method. In this section, the computation of the forces on the inner and outer boundaries of the fluid domain oriented along the direction of bubble translation are obtained using the dissipation approximation, based on irrotational motion. For the outer boundary, in addition to the kinematic constraint imposed on the normal velocity, two choices are considered for the shear stress, as in section 2.2: (i) zero tangential stress and (ii) irrotational tangential stress. Each of these possibilities leads to a set of results that are compared with those from viscous potential flow.

Suppose now that the fluid motion in V is governed by the incompressible Navier−Stokes equations with an appropriate set of boundary conditions that includes expressions 2.2−2.5. The rate of change of kinetic energy in V is

$$\frac{dE}{dt} = \frac{d}{dt}\int_V \rho\frac{|\mathbf{u}|^2}{2} \, dV = \int_V \mathbf{u}\cdot\rho\left(\frac{\partial\mathbf{u}}{\partial t} + \mathbf{u}\cdot\nabla\mathbf{u}\right) dV \tag{2.23}$$

The last equality in constraint 2.23 follows from the fact that mass crosses neither S_1 nor S_2. The fluid has a density ρ and a dynamic viscosity μ. From constraint 2.23, the Navier−Stokes equations and divergence theorem lead to

$$\frac{dE}{dt} = -\int_{S_1} \mathbf{n}_1\cdot\mathbf{T}\cdot\mathbf{u} \, dA + \int_{S_2} \mathbf{n}_2\cdot\mathbf{T}\cdot\mathbf{u} \, dA - \int_V 2\mu\mathbf{D}[\mathbf{u}]:\mathbf{D}[\mathbf{u}] \, dV \tag{2.24}$$

where $\mathbf{T}$ is the stress tensor for a Newtonian fluid and the strain-rate tensor is

$$\mathbf{D}[\mathbf{u}] = \frac{1}{2}(\nabla\mathbf{u} + \nabla\mathbf{u}^T) \tag{2.25}$$

Using expressions 2.1 and 2.7, expression 2.24 leads to

$$UD_1 = -\frac{dE}{dt} - \int_{S_1} \mathbf{n}_1\cdot\mathbf{T}\cdot\mathbf{v} \, dA + \int_{S_2} \mathbf{n}_2\cdot\mathbf{T}\cdot\mathbf{u} \, dA - \int_V 2\mu\mathbf{D}[\mathbf{u}]:\mathbf{D}[\mathbf{u}] \, dV \tag{2.26}$$

Expanding the surface integrals, this expression may be written as

$$UD_1 = -\frac{dE}{dt} - \int_{S_1} \mathbf{n}_1\cdot\mathbf{T}\cdot\mathbf{n}_1(\mathbf{n}_1\cdot\mathbf{v}) \, dA - \int_{S_1} \mathbf{n}_1\cdot\mathbf{T}\cdot\mathbf{t}_1^{(\alpha)}(\mathbf{t}_1^{(\alpha)}\cdot\mathbf{v}) \, dA + \int_{S_2} \mathbf{n}_2\cdot\mathbf{T}\cdot\mathbf{n}_2(\mathbf{n}_2\cdot\mathbf{u}) \, dA + \int_{S_2} \mathbf{n}_2\cdot\mathbf{T}\cdot\mathbf{t}_2^{(\alpha)}(\mathbf{t}_2^{(\alpha)}\cdot\mathbf{u}) \, dA - \int_V 2\mu\mathbf{D}[\mathbf{u}]:\mathbf{D}[\mathbf{u}] \, dV \tag{2.27}$$

With the boundary conditions that are described by expressions 2.2−2.5, we have

$$D_1 = \frac{1}{U}\left(-\frac{dE}{dt} - \int_V 2\mu\mathbf{D}[\mathbf{u}]:\mathbf{D}[\mathbf{u}] \, dV + W\right) \tag{2.28}$$

where

$$W = -\int_{S_1} \mathbf{n}_1\cdot\mathbf{T}\cdot\mathbf{n}_1\hat{q}_1 \, dA + \int_{S_2} \mathbf{n}_2\cdot\mathbf{T}\cdot\mathbf{n}_2 q_2 \, dA + \int_{S_2} \tau_2^{(\alpha)}(\mathbf{t}_2^{(\alpha)}\cdot\mathbf{u}) \, dA \tag{2.29}$$

Expression 2.28 gives the force on S_1 in the $\mathbf{e}_x$-direction due to a Navier−Stokes flow in V satisfying an appropriate set of boundary conditions on S_1 and S_2 that includes those given in expressions 2.2−2.5.

To evaluate the volume integrals in expression 2.28, we now assume that the fluid motion is irrotational, with velocity field $\mathbf{u} = \nabla\phi$. This approximation is satisfactory when the contribution of the rotational component of the fluid motion to the rate of change of kinetic energy and the viscous dissipation is assumed to be small, in comparison to the irrotational contribution. This potential flow is obtained from the solution of the boundary-value problem (expressions 2.13−2.16). Clearly, such potential flow generally cannot satisfy the complete set of boundary conditions that the Navier−Stokes motion does satisfy. With the potential flow assumption, expression 2.23 for the kinetic energy yields

$$\begin{aligned}\frac{dE}{dt} &= \int_V \nabla\cdot\left[\mathbf{u}\rho\left(\frac{\partial\phi}{\partial t} + \frac{|\mathbf{u}|^2}{2}\right)\right] dV = \int_V \nabla\cdot[\mathbf{u}(\rho C(t) - p)] \, dV \\ &= -\int_{S_1} (-p)\mathbf{n}_1\cdot\mathbf{u} \, dA + \int_{S_2} (-p)\mathbf{n}_2\cdot\mathbf{u} \, dA \\ &= -U\int_{S_1} (-p)\mathbf{n}_1\cdot\mathbf{e}_x \, dA - \int_{S_1} (-p)\mathbf{n}_1\cdot\mathbf{v} \, dA + \int_{S_2} (-p)\mathbf{n}_2\cdot\mathbf{u} \, dA\end{aligned} \tag{2.30}$$

with expression 2.16 and $\nabla\cdot u = 0$.

Regarding the dissipation integral, denoting $\mathbf{D} = \mathbf{D}[\mathbf{u} = \nabla\phi]$, one can readily show that, for irrotational motion, the following result holds:

$$\begin{aligned}\int_V 2\mu\mathbf{D}:\mathbf{D} \, dV &= -\int_{S_1} \mathbf{n}_1\cdot 2\mu\mathbf{D}\cdot\mathbf{u} \, dA + \int_{S_2} \mathbf{n}_2\cdot 2\mu\mathbf{D}\cdot\mathbf{u} \, dA \\ &= -U\int_{S_1} \mathbf{n}_1\cdot 2\mu\mathbf{D}\cdot\mathbf{e}_x \, dA - \int_{S_1} \mathbf{n}_1\cdot 2\mu\mathbf{D}\cdot\mathbf{v} \, dA + \int_{S_2} \mathbf{n}_2\cdot 2\mu\mathbf{D}\cdot\mathbf{u} \, dA\end{aligned} \tag{2.31}$$

2.3.1. Zero Tangential Stress on the Outer Boundary. Suppose the outer boundary is also a free surface. Therefore, $\tau_2^{(\alpha)} \equiv 0$ in the last integral of expression 2.29 for W.

The discrepancy between the nonzero irrotational shear stress and the zero shear stress that the Navier−Stokes equations must satisfy at the free surface induces a (viscous) rotational correction to the irrotational normal stress that also enters the computation of the work integrals in expression 2.29. In the

present formulation, this extra stress is ignored. With this assumption, W in expression 2.29 is computed in potential flow:

$$W = -\int_{S_1}(-p + \mathbf{n}_1\cdot 2\mu\mathbf{D}\cdot\mathbf{n}_1)\hat{q}_1\,dA + \int_{S_2}(-p + \mathbf{n}_2\cdot 2\mu\mathbf{D}\cdot\mathbf{n}_2)q_2\,dA \quad (2.32)$$

Therefore, the entire right-hand side of expression 2.28 is furnished by purely irrotational theory and a computable formula for D_1 is obtained.

In inertia-dominated problems, in which viscosity can be regarded as "small" and perturbations of the irrotational motion are confined to narrow boundary layers, evaluating the right-hand side of expression 2.28 from potential flow implies that the viscous contribution to the drag, to first order in the "small" viscosity μ, is assumed to result solely from the rate of energy dissipation, thereby neglecting any possible first-order viscous effect coming from the first and last terms in the right-hand side of expression 2.28.

In the particular case of $\hat{q}_1 = q_2 = 0$, the integrals in expression 2.29 are annihilated and the approximation of W is not an issue. This case represents an extension to a bounded domain of the analysis that was conducted by Joseph, Liao, and Hu[56] and Joseph and Liao,[9] which applies the dissipation approximation to a nonexpanding bubble translating in an unbounded domain.

The substitution of expressions 2.30−2.32 into expression 2.28, after some algebra, yields this expression for the force on the bubble surface in the $\mathbf{e}_x$-direction, according to the dissipation method:

$$D_1 = \int_{S_1}(-p + \mathbf{n}_1\cdot 2\mu\mathbf{D}\cdot\mathbf{n}_1)\mathbf{n}_1\cdot\mathbf{e}_x\,dA + \frac{1}{U}\int_{S_1}\mathbf{n}_1\cdot 2\mu\mathbf{D}\cdot\mathbf{t}_1^{(\alpha)}(\mathbf{t}_1^{(\alpha)}\cdot\mathbf{u})\,dA - \frac{1}{U}\int_{S_2}\mathbf{n}_2\cdot 2\mu\mathbf{D}\cdot\mathbf{t}_2^{(\alpha)}(\mathbf{t}_2^{(\alpha)}\cdot\mathbf{u})\,dA \quad (2.33)$$

To determine the force D_2 on S_2 in the $\mathbf{e}_x$-direction by the dissipation method, we follow a procedure similar to that previously given for D_1, with the difference that the governing equations are transformed to a noninertial reference frame that translates with velocity $U\mathbf{e}_x$. The steps are presented in Appendix A. There, an expression for the force on S_2, with respect to the noninertial frame, is written from the transformed mechanical energy equation. An expression for the force D_2, with respect to the laboratory frame, then can be obtained by evaluating the integrals in potential flow and by employing the transformation rules that link both coordinate systems. The outlined procedure, detailed in Appendix A, results in the relation

$$D_2 = -\int_{S_2}(-p + \mathbf{n}_2\cdot 2\mu\mathbf{D}\cdot n_2)\mathbf{n}_2\cdot\mathbf{e}_x\,dA + \frac{1}{U}\int_{S_2}\mathbf{n}_2\cdot 2\mu\mathbf{D}\cdot\mathbf{t}_2^{(\alpha)}(\mathbf{t}_2^{(\alpha)}\cdot\mathbf{v})\,dA - \frac{1}{U}\int_{S_1}\mathbf{n}_1\cdot 2\mu\mathbf{D}\cdot\mathbf{t}_1^{(\alpha)}(\mathbf{t}_1^{(\alpha)}\cdot\mathbf{v})\,dA \quad (2.34)$$

Next, using expression 2.33 in expression 2.34, with the aid of expression A.23 from Appendix A from the self-equilibration of irrotational viscous stresses, we obtain the net force that must be applied to the liquid system in the $\mathbf{e}_x$-direction:

$$-(D_1 + D_2) = -\int_{S_1}(-p)\mathbf{n}_1\cdot\mathbf{e}_x\,dA + \int_{S_2}(-p)\mathbf{n}_2\cdot\mathbf{e}_x\,dA \quad (2.35)$$

Clearly, the dissipation approximation is an irrotational theory that yields results that are different from those obtained from viscous potential flow in section 2.2. The discrepancy between these two irrotational methods, in the case of an outer free surface, is given by the last two terms in the right-hand side of expressions 2.33 and 2.34.

2.3.2. Irrotational Tangential Stress on the Outer Boundary. The dissipation analysis in section 2.3.1 can be slightly modified to consider an outer surface on which the tangential stress is constrained to be purely irrotational, computed from the solution of the boundary-value problem (expressions 2.13−2.16). A motivation for this alternative outer boundary condition is discussed in section 3.3. In this case, the boundary condition that is described by expression 2.5 becomes

$$\tau_2^{(\alpha)} = \mathbf{n}_2\cdot 2\mu\mathbf{D}\cdot\mathbf{t}_2^{(\alpha)} \quad (2.36)$$

on S_2, where $\mathbf{D} \equiv \nabla\otimes\nabla\phi$. Therefore, no discrepancy exists between the irrotational tangential stress and the tangential stress condition that the Navier−Stokes motion must satisfy. Because of the fact that expression 2.36 holds, the normal component of the stress on S_2 is also irrotational. Therefore, with no approximation, expression 2.29 now takes the form

$$W = -\int_{S_1}\mathbf{n}_1\cdot\mathbf{T}\cdot\mathbf{n}_1\hat{q}_1\,dA + \int_{S_2}(-p + \mathbf{n}_2\cdot 2\mu\mathbf{D}\cdot\mathbf{n}_2)q_2\,dA + \int_{S_2}\mathbf{n}_2\cdot 2\mu\mathbf{D}\cdot\mathbf{t}_2^{(\alpha)}(\mathbf{t}_2^{(\alpha)}\cdot\mathbf{u})\,dA \quad (2.37)$$

This expression is used in expression 2.28. The next step consists of approximating the remaining terms on the right-hand side of expression 2.28 for potential flow that satisy expressions 2.13−2.16. Using expressions 2.30−2.31, the entire analysis therefore leads to

$$D_1 = \int_{S_1}(-p + \mathbf{n}_1\cdot 2\mu\mathbf{D}\cdot\mathbf{n}_1)\mathbf{n}_1\cdot\mathbf{e}_x\,dA + \frac{1}{U}\int_{S_1}\mathbf{n}_1\cdot 2\mu\mathbf{D}\cdot\mathbf{t}_1^{(\alpha)}(\mathbf{t}_1^{(\alpha)}\cdot\mathbf{u})\,dA \quad (2.38)$$

The force D_2 on the outer boundary S_2 is obtained by direct integration of the (irrotational) stresses, using the fact that the viscous irrotational stresses are self-equilibrated on any closed surface (see Appendix B). Thus,

$$D_2 = -\int_{S_2}(-p)\mathbf{n}_2\cdot\mathbf{e}_x\,dA \quad (2.39)$$

Note that the analysis in Appendix A would lead to a different result for the force on S_2 because the zero-tangential-stress boundary condition at the bubble surface would enter the integral analysis in the dissipation approximation, yielding D_2. In contrast, expression 2.39 is an "exact" result obtained here from direct integration over the outer boundary where the stress is known to be irrotational. Therefore, no information from the inner boundary is needed. These formulas are used in the end of section 3.3.

3. Computation of the Forces from the Potential Flow Solution

To compute the forces on the bubble interface and the outer liquid boundary using the formulas obtained in section 2, the solution of the boundary-value problem defined by expressions 2.13−2.16 for the flow is needed. This problem was examined by Sherwood.[55] Because of the fact that he considered an inviscid fluid, the forces were given solely by the irrotational pressure. Since the analysis is explanatory, and for the sake of completeness, a version of Sherwood's analysis is presented

here in section 3.1. The resulting flow field is then used in the computation of the viscous irrotational effects that result in a viscous drag.

3.1. Potential Flow Field. In the bubble-liquid system defined in section 2.1, let R_1 be the radius of the bubble and R_2 be the radius of the outer surface; also, let ϵ be the separation between the centers of the bubble and the outer sphere. The translational velocity then is given as $U = \dot{\epsilon}$. Recall that the center of the bubble moves along the fixed direction $\mathbf{e}_x$, and its pathline contains the center of the outer envelope, thereby defining the axis of symmetry for the flow field. According to the notation defined in section 2, the bubble interface and the outer sphere are denoted as S_1 and S_2, respectively. The analysis that follows intends to predict the forces exerted by the liquid on the bubble and the outer container along the $\mathbf{e}_x$-direction for $\epsilon = 0$. Therefore, the analysis is conducted for $\epsilon/R_1 \ll 1$ and $\epsilon/R_1 \ll R_2/R_1 - 1$.

The volume occupied by the liquid for all time is $4\pi(R_2^3 - R_1^3)/3$. Then,

$$R_1^{\,2}\dot{R}_1 = R_2^{\,2}\dot{R}_2 \tag{3.1}$$

where the dot above the variable denotes time differentiation. Using spherical polar coordinates (r, θ) with orthonormal basis $\{\mathbf{e}_r, \mathbf{e}_\theta\}$, and the center of S_2 given by $r = 0$, the bubble surface is described by

$$r = \epsilon\cos\theta + R_1\left[1 - \left(\frac{\epsilon}{R_1}\right)^2\sin^2\theta\right]^{1/2} \tag{3.2}$$

Expanding around $\epsilon = 0$,

$$r = R_1 + \epsilon\cos\theta + O(\epsilon^2) \tag{3.3}$$

The harmonics velocity potential ϕ that gives rise to an axisymmetric flow field is

$$\phi = \frac{B_0}{r} + \sum_{l=1}^{\infty}(A_l r^l + B_l r^{-l-1})P_l(\cos\theta) \tag{3.4}$$

such that $u = \nabla\phi$. In expression 3.4, P_l denotes the Legendre polynomial of degree l (see Strauss,[57] p 275). This potential must satisfy the boundary conditions

$$\mathbf{n}_1\cdot\nabla\phi\Big|_{S_1} = q_1 = U\mathbf{n}_1\cdot\mathbf{e}_x + \hat{q}_1 = \dot{R}_1 + \dot{\epsilon}\cos\theta - \frac{\epsilon\dot{\epsilon}}{R_1}\sin^2\theta + O(\varepsilon^2) \tag{3.5}$$

and

$$\mathbf{n}_2\cdot\nabla\phi\Big|_{S_2} = q_2 = \dot{R}_2 \tag{3.6}$$

where $\hat{q}_1 = \dot{R}_1$ and, to first order in ϵ,

$$\mathbf{n}_1 = \mathbf{e}_r + \mathbf{e}_\theta\left(\frac{\varepsilon}{R_1}\right)\sin\theta \tag{3.7}$$

and $\mathbf{n}_2 = \mathbf{e}_r$. The boundary condition defined by expression 3.6 yields

$$B_0 = -R_2^{\,2}\dot{R}_2 = -R_1^{\,2}\dot{R}_1 \tag{3.8}$$

and

$$A_l R_2^{\,l-1} = B_l(l+1)R_2^{\,-l-2} \qquad (\text{for } l \geq 1) \tag{3.9}$$

With the potential given in expression 3.4, the velocity field components in the (r, θ) frame are obtained: $\mathbf{u} = \mathbf{e}_r u_r + \mathbf{e}_\theta u_\theta = \mathbf{e}_r\,\partial\phi/\partial r + \mathbf{e}_\theta\partial\phi/r\,\partial\theta$.

Turning to the bubble surface S_1, the boundary condition described by expression 3.5 allows us to find the coefficients in expression 3.4. In so doing, it is convenient to expand these coefficients as a power series in ϵ. That is,

$$A_l = A_l^{(0)} + A_l^{(1)}\epsilon + A_l^{(2)}\epsilon^2 + \cdots, \qquad B_l = B_l^{(0)} + B_l^{(1)}\epsilon + B_l^{(2)}\epsilon^2 + \cdots \tag{3.10}$$

for $l \geq 1$, where $A_l^{(j)}$ and $B_l^{(j)}$ are related through expression 3.9. Sherwood[55] obtained, for $l = 1$,

$$A_1 = -\frac{R_1^{\,3}(\dot{\varepsilon} + 2\varepsilon\dot{R}_1R_1^{\,-1})}{R_2^{\,3} - R_1^{\,3}}, \quad B_1 = -\frac{R_1^{\,3}R_2^{\,3}(\dot{\varepsilon} + 2\varepsilon\dot{R}_1R_1^{\,-1})}{2(R_2^{\,3} - R_1^{\,3})} \tag{3.11}$$

to first order in ϵ. Some detail on the computations of these coefficients by imposing constraint 3.5 is given in Appendix C, where expressions for A_2 and B_2, to leading order, are also presented. There, we also show that $A_l^{(0)} = B_l^{(0)} = 0$ for $l \geq 2$ and that $A_l^{(1)} = B_l^{(1)} = 0$ for $l \geq 3$. Because the forces on S_1 and S_2 in the $\mathbf{e}_x$-direction are computed for $\epsilon = 0$, it suffices to find the coefficients B_0, A_1, B_1, A_2, and B_2 to first order in ϵ and then calculate their time derivatives. However, these computations will show that only $l = 1$ terms—and, thus, A_1 and B_1—are actually needed, because of the orthogonality properties of Legendre polynomials.

The fluid pressure p distribution on S_1 and S_2 can be obtained from the Bernoulli equation (expression 2.16). The derivative $\partial\phi/\partial t$, which is needed to compute p, is obtained from expression 3.4 by differentiating the coefficients and then putting $\epsilon = 0$, with $r = R_1$ or $r = R_2$.

Using standard formulas, the components of the strain-rate tensor in spherical-polar coordinates can be computed from $\mathbf{u} = \nabla\phi$, with ϕ given by expression 3.4. These computations yield

$$D_{rr} = \mathbf{e}_r\cdot 2\mu\mathbf{D}[\nabla\phi]\cdot\mathbf{e}_r = \sum_{l=0}^{\infty}[l(l-1)A_l r^{l-2} + (l+1)(l+2)B_l r^{-l-3}]P_l(\cos\theta) \tag{3.12}$$

$$D_{r\theta} = \mathbf{e}_r\cdot 2\mu D[\nabla\phi]\cdot\mathbf{e}_\theta = \sum_{l=1}^{\infty}[(l-1)A_l r^{l-2} - (l+2)B_l r^{-l-3}]\frac{\mathrm{d}P_l(\cos\theta)}{\mathrm{d}\theta} \tag{3.13}$$

For $\epsilon = 0$, at $r = R_1$, the velocity component u_r is given by expression 3.5 and the component u_θ is given as $u_\theta = \partial\phi/r\,\partial\theta$; hence,

$$u_r = \dot{R}_1 + \dot{\varepsilon}\cos\theta, \quad u_\theta = -(A_1 + B_1R_1^{\,-3})\sin\theta \tag{3.14}$$

At $r = R_2$, with $\epsilon = 0$, $u_r = \partial\phi/\partial r$ and $u_\theta = \partial\phi/r\,\partial\theta$ give

$$u_r = -B_0R_2^{\,-2}, \quad u_\theta = -(A_1 + B_1R_2^{\,-3})\sin\theta \tag{3.15}$$

With $\epsilon = 0$, evaluating expressions 3.12 and 3.13 at $r = R_1$ yields

$$D_{rr} = 2B_0R_1^{\,-3} + 6B_1R_1^{\,-4}\cos\theta, \quad D_{r\theta} = 3B_1R_1^{\,-4}\sin\theta \tag{3.16}$$

and, at $r = R_2$, we have

$$D_{rr} = 2B_0R_2^{\,-3} + 6B_1R_2^{\,-4}\cos\theta, \quad D_{r\theta} = 3B_1R_2^{\,-4}\sin\theta \tag{3.17}$$

In these results, B_0 is given by expression 3.8 and A_1 and B_1 are given in expression 3.11 with $\epsilon = 0$. Note that the alternative

approach of computing the velocity potential from a boundary-value problem that considers two instantaneously growing or collapsing concentric spheres would have sufficed to obtain the strain-rate tensor $D[\nabla\phi]$, because it only involves spatial partial differentiation.

Below, the forces on the bubble interface S_1 and the outer boundary S_2 are computed from the formulas of this section and section 2 for $\epsilon = 0$. When the bubble and the outer surface are concentric, $\mathbf{n}_1 = \mathbf{n}_2 = \mathbf{e}_r$, $\mathbf{t}_1 = \mathbf{t}_2 = \mathbf{e}_\theta$, with $\mathbf{e}_r \cdot \mathbf{e}_x = \cos\theta$ and $\mathbf{e}_\theta \cdot \mathbf{e}_x = -\sin\theta$.

3.2. Forces—Viscous Potential Flow. The force on the bubble according to viscous potential flow is computed from expression 2.18. For the spherical bubble, with $\epsilon = 0$ at $r = R_1$, this expression becomes

$$D_1 = 2\pi R_1^2 \int_0^\pi (-p + 2\mu D_{rr})\Big|_{R_1} \cos\theta \sin\theta \, d\theta \quad (3.18)$$

With the Bernoulli equation (expression 2.16), computing $\partial\phi/\partial t$, and using expressions 3.14 and 3.16, we get

$$D_1 = -\frac{4}{3}\pi\rho {R_1}^3 \left[\frac{\ddot{\epsilon}({2R_1}^3 + {R_2}^3)}{2({R_2}^3 - {R_1}^3)} + \frac{\dot{\epsilon}\dot{R}_1(15{R_1}^3 + 3{R_2}^3)}{2R_1({R_2}^3 - {R_1}^3)} + \frac{6\nu\dot{\epsilon}}{{R_1}^2}\frac{{R_2}^3}{({R_2}^3 - {R_1}^3)} \right] \quad (3.19)$$

Taking $R_2 \to \infty$, this expression leads to

$$D_1 = -\frac{4}{3}\pi\rho {R_1}^3 \left[\frac{\ddot{\epsilon}}{2} + \frac{3\dot{\epsilon}\dot{R}_1}{2R_1} + \frac{6\nu\dot{\epsilon}}{{R_1}^2} \right] \quad (3.20)$$

In particular, for a spherical bubble of constant volume that translates with constant velocity (i.e., $\dot{R}_1 = 0$ and $\ddot{\epsilon} = 0$), expression 3.20 reduces to $D_1 = -8\pi\mu\dot{\epsilon}R_1$, which is a result Moore determined in 1959 from direct integration of the viscous normal stress in irrotational motion.[15] If the fluid is considered inviscid, then the drag is zero (d'Alembert's paradox). When the acceleration $\ddot{\epsilon}$ is not zero, expression 3.20 results in the apparent mass.

With $\dot{R}_1 = 0$ and the void fraction $\alpha = (R_1/R_2)^3$, expression 3.19 reduces to

$$D_1 = -\frac{4}{3}\pi\rho {R_1}^3 \left[\frac{\ddot{\epsilon}(1 + 2\alpha)}{2(1 - \alpha)} + \frac{6\nu\dot{\epsilon}}{{R_1}^2}\frac{1}{(1 - \alpha)} \right] \quad (3.21)$$

which is in agreement, when $\nu = 0$, with eq AI.11 of Zuber[58] for the force on a spherical bubble moving within an inviscid liquid bounded by a spherical shell. This leads to the cell void fraction correction of the accelerated-apparent mass given in expression 3.20.

For "small" values of α, it is useful to write expression 3.21 in the form

$$D_1 = -\frac{4}{3}\pi\rho {R_1}^3 \left[\frac{\ddot{\epsilon}}{2}(1 + 3\alpha) + \frac{6\nu\dot{\epsilon}}{{R_1}^2}(1 + \alpha) \right] + O(\alpha^2) \quad (3.22)$$

The force on the outer sphere, $r = R_2$, with $\epsilon = 0$, is obtained from expression 2.19 when the outer boundary is a free surface. This yields

$$D_2 = -2\pi {R_2}^2 \int_0^\pi (-p + 2\mu D_{rr})\Big|_{R_2} \cos\theta \sin\theta \, d\theta \quad (3.23)$$

Finding $\partial\phi/\partial t$, with expressions 3.15 and 3.17, this formula gives

$$D_2 = \frac{4}{3}\pi\rho {R_2}^3 \left[\frac{3\ddot{\epsilon}{R_1}^3}{2({R_2}^3 - {R_1}^3)} + \frac{\dot{\epsilon}{R_1}^2\dot{R}_1(15{R_2}^3 + 3{R_1}^3)}{2{R_2}^3({R_2}^3 - {R_1}^3)} + \frac{6\nu\dot{\epsilon}}{{R_2}^2}\frac{{R_1}^3}{({R_2}^3 - {R_1}^3)} \right] \quad (3.24)$$

Using expressions 3.19 and 3.24, the total force that must be applied to the system is

$$-(D_1 + D_2) = -\frac{4}{3}\pi\rho {R_1}^3 \left[\ddot{\epsilon} + \frac{6\dot{\epsilon}\dot{R}_1}{R_1} - \frac{6\nu\dot{\epsilon}}{{R_1}^2}\frac{R_2({R_2}^2 - {R_1}^2)}{({R_2}^3 - {R_1}^3)} \right] \quad (3.25)$$

For $\nu = 0$ (inviscid fluid), these results are reduced to those obtained by Sherwood.[55] The force D_2 when the irrotational stress is specified on S_2 is given by expression 3.24 with $\nu = 0$. This follows from expression 2.22.

3.3. Forces—Dissipation Method. The force D_1 on the bubble interface S_1 in the $\mathbf{e}_x$-direction can be obtained using expression 2.33 when a zero shear stress is prescribed on the outer boundary. This formula can be written as

$$D_1 = 2\pi R_1^2 \int_0^\pi (-p + 2\mu D_{rr})\Big|_{R_1} \cos\theta \sin\theta \, d\theta + \frac{2\pi {R_1}^2}{\dot{\epsilon}} \int_0^\pi (2\mu D_{r\theta} u_\theta)\Big|_{R_1} \sin\theta \, d\theta - \frac{2\pi {R_2}^2}{\dot{\epsilon}} \int_0^\pi (2\mu D_{r\theta} u_\theta)\Big|_{R_2} \sin\theta \, d\theta \quad (3.26)$$

With expression 2.16 for the pressure, and expressions 3.14 and 3.16, expression 3.26 leads to

$$D_1 = -\frac{4}{3}\pi\rho {R_1}^3 \left[\frac{\ddot{\epsilon}({2R_1}^3 + {R_2}^3)}{2({R_2}^3 - {R_1}^3)} + \frac{\dot{\epsilon}\dot{R}_1(15{R_1}^3 + 3{R_2}^3)}{2R_1({R_2}^3 - {R_1}^3)} + \frac{9\nu\dot{\epsilon}}{{R_1}^2}\frac{R_2({R_2}^5 - {R_1}^5)}{({R_2}^3 - {R_1}^3)^2} \right] \quad (3.27)$$

This expression, with $R_2 \to \infty$, reduces to

$$D_1 = -\frac{4}{3}\pi\rho {R_1}^3 \left[\frac{\ddot{\epsilon}}{2} + \frac{3\dot{\epsilon}\dot{R}_1}{2R_1} + \frac{9\nu\dot{\epsilon}}{{R_1}^2} \right] \quad (3.28)$$

For a spherical bubble of constant volume moving with constant velocity $\dot{\epsilon}$ in an infinite fluid, expression 3.28 gives $D_1 = -12\pi\mu\dot{\epsilon}R_1$. This result has been obtained with the dissipation method in potential flow by several authors.[8−12,14,56]

Moore[12] has examined the discrepancy between the viscous potential flow solution and the correct dissipation result for the drag over a spherical bubble of constant volume translating in an unbounded domain. Moore explained, citing an idea that was due to G. K. Batchelor, that the addition of an extra pressure or viscous correction to the irrotational normal stress can compensate for such a discrepancy. From a boundary-layer type of analysis that assesses the order of magnitude of the various terms in the steady governing equations, Moore concluded that the extra pressure "contributes to the drag on the bubble to the same order as the viscous stresses",[12] because he found that this extra pressure is first order in the dimensionless viscosity. If the extra-pressure produces work, this is evidently neglected in the approach used here (that is, for nonzero choices of $\hat{q}_1$ and q_2), for W in expression 2.29 is approximated by the irrotational pressure and irrotational viscous normal stress.

For a bubble of variable radius in an unbounded fluid, the viscous part in expression 3.28 can be reduced from the multiple-bubble analysis by Voinov and Golovin.[25] They applied a Lagrangian formulation to examine the motion of a set of N bubbles of varying radius translating in a liquid otherwise at rest with dissipative forces computed from the rate of viscous dissipation evaluated in potential flow. Magnaudet and Legendre[18] obtained expression 3.28 by transforming the original problem to a reference frame in which the bubble radius remains fixed, while preserving the dynamic similarity in the transformation. In the limit when $Re \gg 1$ or $\mathscr{U}Re \gg 1$, where the Reynolds number is $Re = R_1U/\nu$ and the velocity ratio $\mathscr{U} = |\dot{R}_1|U$, the boundary layer is thin. The transformed problem thus involves a bubble of constant radius in an unsteady flow and the drag force is computed to first order in the viscosity by evaluating the kinetic energy and the viscous dissipation from potential flow (see Tam[16]). The force in physical space is then found by simply applying the known rules that link the transformed problem to the original one. This method contrasts with the approach described in section 2.3, which results in expression 3.28, in which the work of the normal stress due to the radial motion of the bubble interface and the contribution of this motion to the liquid kinetic energy are modeled by potential flow in a rather heuristic way. The fact that expression 3.28 agrees with the force given by Magnaudet and Legendre[18] indicates that the combined viscous contribution from $\mathrm{d}E/\mathrm{d}t$ and W in expression 2.28 is null up to order $O(Re^{-1})$. This may be explained by considering that the component of the total motion attributed to the bubble radial expansion and contraction is of the source-sink type and, hence, of an irrotational nature.

The result obtained above can be readily used to approximate the dynamics in a bubble swarm with a void fraction α by applying the cell model described in section 1. In the case of $\dot{R}_1 = 0$, with the cell void fraction, $\alpha = (R_1/R_2)^3$ (see expression 3.27), gives the added mass and viscous contributions to the force acting on each bubble:

$$D_1 = -\frac{4}{3}\pi\rho {R_1}^3\left[\frac{\ddot{\epsilon}(1+2\alpha)}{2(1-\alpha)} + \frac{9\nu\dot{\epsilon}}{{R_1}^2}\frac{(1-\alpha^{5/3})}{(1-\alpha)^2}\right] \quad (3.29)$$

This result agrees with that of Zuber[58] for $\nu = 0$. The viscous part in expression 3.29 is the widely cited result that is obtained with the dissipation approximation by Marrucci.[51] For "'small" values of α, expression 3.29 may be written as

$$D_1 = -\frac{4}{3}\pi\rho {R_1}^3\left[\frac{\ddot{\epsilon}}{2}(1+3\alpha) + \frac{9\nu\dot{\epsilon}}{{R_1}^2}(1+2\alpha)\right] + O(\alpha^2) \quad (3.30)$$

Note that expression 3.29 has been derived from a cell model with a frictionless outer boundary, so that no work is exchanged by the reference cell with the surroundings.

The force D_2 in the $\mathbf{e}_x$-direction on surface S_2 can be obtained from either expression 2.34 or 2.35. The latter expression can be written as

$$D_1 + D_2 = 2\pi {R_1}^2\int_0^\pi (-p)\Big|_{R_1}\cos\theta\sin\theta\,\mathrm{d}\theta - 2\pi {R_2}^2\int_0^\pi (-p)\Big|_{R_2}\cos\theta\sin\theta\,\mathrm{d}\theta \quad (3.31)$$

which, with expression 3.27, leads to

$$D_2 = \frac{4}{3}\pi\rho {R_2}^3\left[\frac{3\ddot{\epsilon}{R_1}^3}{2({R_2}^3 - {R_1}^3)} + \frac{\dot{\epsilon}{R_1}^2\dot{R}_1(15{R_2}^3 + 3{R_1}^3)}{2{R_2}^3({R_2}^3 - {R_1}^3)} + \frac{9\nu\dot{\epsilon}\,R_1({R_2}^5 - {R_1}^5)}{{R_2}^2({R_2}^3 - {R_1}^3)^2}\right] \quad (3.32)$$

Again, Sherwood's results are recovered, taking $\nu = 0$ in expressions 3.27 and 3.32.

The total force that must be applied to the system is obtained from expression 3.31:

$$-(D_1 + D_2) = -\frac{4}{3}\pi\rho {R_1}^3\left(\ddot{\epsilon} + \frac{6\dot{\epsilon}\dot{R}_1}{R_1}\right) \quad (3.33)$$

which is consistent with the inviscid result by Sherwood.[55]

Consider now an outer boundary S_2 in which the tangential stress is given by the irrotational motion satisfying the boundary-value problem (see expressions 2.13−2.16), such that the zero-tangential-stress constraint does not hold. Under this framework, the formulas of section 2.3.2 can be applied yielding an expression for the force D_1 on the bubble and the force D_2 on the outer spherical envelope. Applying expression 2.38, we obtain

$$D_1 = -\frac{4}{3}\pi\rho {R_1}^3\left[\frac{\ddot{\epsilon}(2{R_1}^3 + {R_2}^3)}{2({R_2}^3 - {R_1}^3)} + \frac{\dot{\epsilon}\dot{R}_1(15{R_1}^3 + 3{R_2}^3)}{2R_1({R_2}^3 - {R_1}^3)} + \frac{9\nu\dot{\epsilon}}{{R_1}^2}\frac{{R_2}^6}{({R_2}^3 - {R_1}^3)^2}\right] \quad (3.34)$$

With $\dot{R}_1 = 0$, in terms of the void fraction α, this expression becomes

$$D_1 = -\frac{4}{3}\pi\rho {R_1}^3\left[\frac{\ddot{\epsilon}(1+2\alpha)}{2(1-\alpha)} + \frac{9\nu\dot{\epsilon}}{{R_1}^2}\frac{1}{(1-\alpha)^2}\right] \quad (3.35)$$

To first order in α, expression 3.35 also leads to expression 3.30. The viscous part of expression 3.35 has been given by Kendoush,[52] as discussed below. The force D_2, according to expression 2.39, can be obtained from either expression 3.24 or expression 3.32, taking $\nu = 0$. For the two outer boundary conditions examined here, note that the force on the bubble increases with the void fraction, according to both irrotational theories.

4. Discussion

The force acting on a spherical compressible bubble in rectilinear motion within an incompressible fluid bounded externally by a spherical surface has been computed above at the instant in which both spheres are concentric. The analysis is performed using two different irrotational approximations, namely, viscous potential flow (sections 2.2 and 3.2), which directly integrates the irrotational normal stress over the bubble surface, and the dissipation method (sections 2.3 and 3.3), in which the integration of the various terms in the mechanical energy equation, including the rate of energy dissipation, is performed assuming irrotational motion, after satisfying actual boundary conditions for Navier−Stokes motion. The dissipation method stems from the fact that viscous irrotational stresses are self-equilibrated, but its power does not vanish.[59] In addition, the force on the outer surface is also computed. In particular, by keeping the bubble radius constant, one can use the results to approach the force on a bubble moving in a monodispersed homogeneous bubbly liquid that has the same void fraction as the reference cell and satisfies the dual limit of large Re and

small *We*, because, in this case, the velocity field differs very little from that in irrotational motion. This is in accord with the well-known cell-model approximation.

In the present formulation of the dissipation method, the tangential stress is set to zero on the inner boundary, but two possibilities are considered for the outer boundary: either a zero tangential stress or an irrotational tangential stress. Because the irrotational tangential stress on the outer boundary is not identically zero, this stress does work against the remainder of the domain, as shown in expression 2.37. Therefore, this boundary condition contradicts the postulate by Happel and Brenner[45] of regarding each cell as an independent entity in the sense that energy transfer should not occur between the unit cell and the neighboring fluid. This is the case with the model with zero tangential stress on both the inner and outer boundaries (i.e., free-surface cell model), leading to Marrucci's drag when the bubble speed is constant. Nevertheless, if the cell model is used to describe a bubbly suspension with "weak" rotational effects confined to a thin layer adjacent to the bubble interface and a minute wake at the bubble rear, such that the liquid motion is essentially irrotational, the choice of irrotational stresses on the outer envelope seems reasonable.

The viscous drag from the viscous potential flow solution (expression 3.21) is always less than the viscous drag obtained from the dissipation method with either outer boundary condition (expression 3.29 or 3.35) for the same volume fraction α. It is well-known[12] that the drag on a single bubble rising steadily in a liquid from the integration of the viscous irrotational normal stress (i.e., viscous potential flow in this paper) is two-thirds of that predicted by the dissipation method, which gives the correct trend for a large-*Re* spherical bubble. Therefore, one may expect the results from the dissipation method to be closer to the actual viscous drag than those from viscous potential flow for nonzero α.

For a bubble moving with constant velocity, i.e., $\ddot{\epsilon} = 0$, expression 3.35 reduces to the drag found by Kendoush[52] with the dissipation method using a cell model. Nonetheless, in his analysis, the dynamic constraint (stress) at the outer boundary is not stated. Expression 3.34 and, hence, expression 3.35, were attained here by imposing an irrotational tangential stress on the outer boundary. Both Marruci[51] and Kendoush[52] used the irrotational velocity profile determined by the domain configuration and the kinematic conditions (normal velocity component) on the inner and outer boundaries. Kendoush's working equation (eq 5 in his work) can be obtained from expression 2.38, using expression 2.1.

Kendoush also argued that Marrucci's result, given in expression 3.29 for $\ddot{\epsilon} = 0$, was incorrect, reasoning that the upper integration limit in Marrucci's dissipation integral should have been taken to infinity instead of using the outer radius, as originally specified by Marrucci. Although implementing this change in Marrucci's formulation does lead to expression 3.35 instead of expression 3.29, we find this modification rather contradictory, because, in the cell model, the liquid is bounded, and the velocity profile employed is that of a confined fluid. The analysis that led to expression 3.29 verifies that Marrucci's formula for the viscous drag is correct; it is found here from the mechanical energy balance by considering frictionless inner and outer boundaries and irrotational motion in the bulk of fluid. Note that Marrucci did not prescribe any external boundary condition from the dynamics (i.e., stress), although he did mention Happel's[48] assumption of a free-surface condition for the outer boundary in a creeping-flow cell model as a prominent antecedent of his work. He only indicates that boundary-layer contributions to the total energy dissipation are neglected in his analysis.

While a zero tangential stress is the obvious choice for the bubble interface, an alternative constraint—that is, an irrotational stress condition—may be specified on the outer boundary. In summary, expressions 3.29 and 3.35 result from the dissipation method applied to the same configuration with the same frictionless condition on the inner boundary but with each satisfying a different condition on the outer boundary, thereby yielding different results. Nonetheless, the drag is the same to first order in the void fraction.

4.1. Comparison with Numerical and Other Analytical Results. The viscous irrotational theories considered here can be compared with results from other analytical models, numerical simulations, and experimental data. We have in mind the situation of gas being bubbled through a stagnant liquid in a continuous manner by injecting a constant gas flow rate or the case of a swarm of spherical bubbles rising by buoyancy in a liquid otherwise at rest. The latter case can be placed in the framework of the cell-model analysis conducted here by letting U be the velocity of the rising bubble swarm, with respect to the container wall.[51,53] If a steady gas flow rate is bubbled through the same container, the actual bubble velocity U_b referred to the container walls is related to U by the expression $U_b = U/(1 - \alpha)$, as a result of mass conservation,[60] where α is also the gas volume fraction in the bubbly flow. In this case, U also represents the gas drift velocity, that is, the difference between the actual gas velocity (U_b) and the gas volumetric flow rate per unit of cross-sectional area being pushed into the system.[60] It is assumed that the bubbles in the swarm are almost spherical, homogeneously distributed, and with negligible variations of the equivalent bubble diameter, with respect to the mean value. The equivalent bubble diameter is the diameter of the sphere with the same volume of the bubble. We are referring to this definition when we use the term "bubble diameter".

In Figure 2a, the predictions by the irrotational theories for the drag coefficient C_D are presented and compared with those listed in Chhabra[46] from the numerical solution of the steady incompressible Navier−Stokes equations, using both the free-surface and the zero-vorticity cell-model approximations for $Re = 100$, where $Re = 2R_1U\rho/\mu$, thereby making it suitable for comparison with the viscous irrotational theories. Numerical results for $Re = 20$ are also included, to illustrate the change in C_D with *Re*. Chhabra collected the results obtained by Manjunath et al.,[54] using the finite-element method for a cell model with zero tangential stress both on the inner and outer boundary and new results generated with the same numerical method solving the governing equations for the same physical domain and boundary conditions, except that, at the outer boundary, the vorticity is set to zero instead of the tangential stress. The drag D on a bubble may be written in the form

$$D = \frac{1}{2}\rho U^2 \pi R_1^{\,2} C_D \tag{4.1}$$

This is an expression that defines the drag coefficient C_D. Using the results for the viscous drag from expressions 3.21, 3.29, and 3.35, expressions for the drag coefficient can thus be written, respectively, for viscous potential flow (VPF) and the dissipation method (DM) with either a zero tangential stress or an irrotational tangential stress on the outer boundary. In this order, we obtain

$$C_{D_1} = \frac{32}{Re}\frac{1}{(1 - \alpha)} \tag{4.2.a}$$

$$C_{D_2} = \frac{48}{Re}\frac{(1-\alpha^{5/3})}{(1-\alpha)^2} \tag{4.2.b}$$

$$C_{D_3} = \frac{48}{Re}\frac{1}{(1-\alpha)^2} \tag{4.2.c}$$

Figure 2a shows that the DM with the irrotational-tangential-stress condition on the outer boundary exhibits fair agreement with the numerical results for the zero-vorticity cell model for the range of void fraction considered in the study. In this formulation of the dissipation approximation, the potential flow hypothesis is brought from the bulk of the fluid to include the outer boundary. Predictions from the DM with the zero-tangential-stress condition on the outer surface are similar to the numerical simulations using a cell model with the same constraint, as expected for $Re = 100$. VPF, on the other hand, consistently underpredicts the numerical solution, which is the extension to a bubbly suspension of the known result for a single bubble rising in an infinite medium.[12] From the two curves rendered by DM, the cell model with an irrotational shear stress on the outer boundary predicts values for the drag coefficient C_D that display a stronger dependence on the void fraction than those from the cell model with a zero-shear-stress condition. A similar trend is described by the numerical results by Chhabra,[46] who commented on this, for $Re = 100$ (represented by symbols); that is, results from the zero-vorticity cell model are more dependent on the void fraction than results from the free-surface cell model. This trend agrees with that reported by Happel and Brenner[45] and El-Kaissy and Homsy.[50] Happel and Brenner[45] framed their discussion under the analysis of creeping flow; El-Kaissy and Homsy[50] applied regular perturbation techniques on the Navier−Stokes equations. A comparison of numerical predictions for the drag coefficient with Marrucci's drag (cf. expression 4.2.b) has been presented by Manjunath et al.,[54] using the free-surface cell model.

Although numerical simulations and analytical models can predict the drag that acts on a bubble in a bubbly suspension, perhaps the most convenient way of evaluating their performance is comparison of the theoretical results for the terminal rise velocity of the bubbles with experimental data. This is because measurements of this magnitude are somewhat abundant in the literature. The terminal velocity U of a swarm of spherical bubbles of equal size rising due to buoyancy can be determined by equating the drag on a bubble with the lift force that drives the bubble upward, given by the buoyancy force corrected by the bubble weight, that is, $4\pi R_1^3(\rho_M - \rho_G)g/3$, with g being the acceleration of gravity, ρ_G the gas density, and ρ_M the average density of the mixture ($\rho_M \equiv \rho(1-\alpha) + \rho_G\alpha$).[52,58,61] Using expressions 3.21, 3.29, and 3.35 for the drag, we thus find

$$\frac{U}{U_\infty} = \frac{3}{2}(1-\alpha)^2 \tag{4.3.a}$$

$$\frac{U}{U_\infty} = \frac{(1-\alpha)^3}{(1-\alpha^{5/3})} \tag{4.3.b}$$

$$\frac{U}{U_\infty} = (1-\alpha)^3 \tag{4.3.c}$$

for VPF, and the DM with either a zero tangential stress or an irrotational tangential stress at the outer boundary of the cell, respectively. Here, U_∞ is the bubble velocity in the limit of infinite dilution (that is, for $\alpha = 0$), computed from the DM,[1] $U_\infty = R_1^2(\rho - \rho_G)g/(9\mu)$. Hence, the bubble rise velocity for infinite dilution according to VPF is $3U_\infty/2$. Expression 4.3.c has been given by Kendoush.[52] Expression 4.3.b multiplied by the factor $(1-\alpha)^{-1}$ gives the rise velocity model described by Marrucci,[51] who apparently used the density of the liquid ρ instead of the density of the mixture ρ_M in the buoyancy force. Richardson and Zaki[62] favored the use of the density of the liquid over the density of the suspension ρ_M in computing the buoyancy force that acts on solid particles settling in a liquid at the same rate, pointing out that each particle displaces its own volume of liquid, not a volume of suspension. Kuwabara[49] also used the density of the liquid instead of that of the suspension for the buoyancy force needed in the evaluation of the terminal settling velocity of spheres uniformly arranged in a liquid. Manjunath et al.[54] proposed to compute the steady rise velocity of the bubble swarm with the buoyancy force determined by the density of the liquid. On the other hand, Zuber[58] applied the one-dimensional momentum equation for two-phase flow to the case of steady vertical motion of particles in a fluid, neglecting the friction at the walls, finding that the buoyancy force determined with the density of the mixture balances the drag force on a particle and its weight. Based on experimental studies on the settling velocity of spheres in two-component solid−liquid suspensions, Poletto and Joseph[63] affirmed that the effective density approaches the average density of the mixture in the case of a test particle of the same diameter as the suspended particles, or larger. Moreover, they entered the average density of the mixture to account for the effective buoyancy on a test particle in a model describing the settling of a test sphere in a suspension. Kendoush also used the density of the mixture in finding the terminal rise velocity of a bubble swarm. This approach was adopted above.

Expressions 4.3.a−4.3.c are plotted in Figure 2b, as functions of the void fraction. To use the numerical results for C_D that were compiled in the work by Chhabra[46] for fixed Reynolds number Re and varying α to predict the ratio U/U_∞, the drag D in expression 4.1 is equated to the buoyancy force minus the bubble weight. That is,

$$C_D\frac{1}{2}\rho U^2\pi {R_1}^2 = \frac{4}{3}\pi {R_1}^3(\rho - \rho_G)g(1-\alpha) \tag{4.4}$$

Writing a similar expression in the infinite dilution limit, $\alpha = 0$, for a bubble of radius R_1 rising with velocity U_∞ in the same liquid, according to the dissipation method, the drag coefficient being $C_{D,\infty}$, and combining with expression 4.4, we find[64]

$$\frac{U}{U_\infty} = (1-\alpha)^{1/2}\left(\frac{C_{D,\infty}}{C_D}\right)^{1/2} \tag{4.5}$$

With $C_{D,\infty}$ given by the known expression $C_{D,\infty} = 48/Re_\infty$, and $U/U_\infty = Re/Re_\infty$, expression 4.5 represents an implicit relation for Re_∞, for known values of α and Re, which are a pair that determines the drag coefficient C_D from the numerical analysis. Expression 4.5 can be written in explicit form:

$$\frac{U}{U_\infty} = (1-\alpha)\frac{48}{ReC_D} \tag{4.6}$$

The results from expression 4.6 for $Re = 20$ and 100 are represented with symbols in Figure 2b.

The trend depicted by the viscous irrotational theories in Figure 2b indicates a decrease in the ratio U/U_∞ for the bubble swarm with increasing void fraction. For a given gas−liquid system for which the dual limit of large Re and small We is satisfied, this trend indicates that increasing bubble concentration hinders the bubble swarm rise speed. DM with an irrotational tangential stress on the outer boundary of the cell

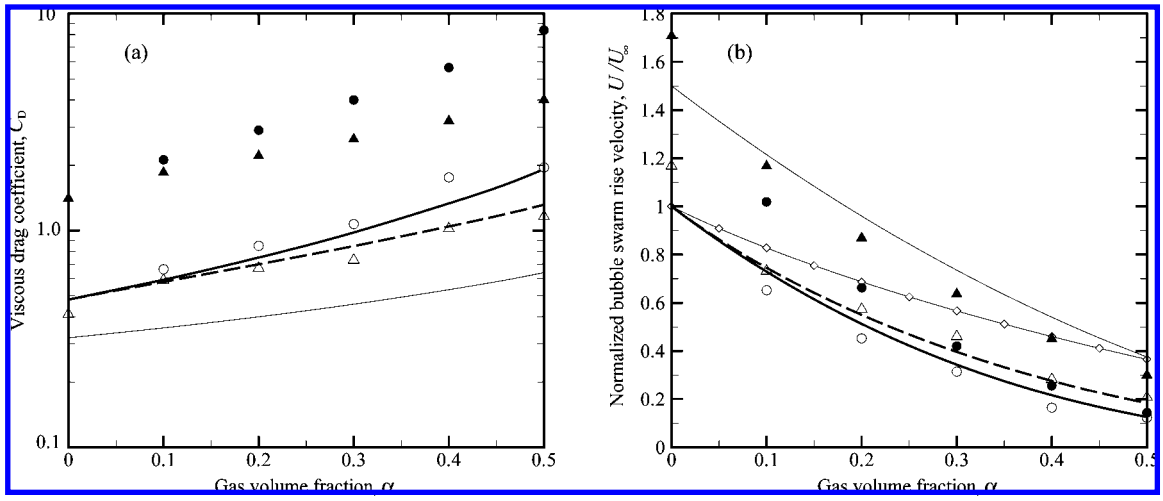

Figure 2. Graphs showing (a) the drag coefficient (C_D), as a function of the void fraction (α), and (b) the normalized bubble swarm rise velocity (U/U_∞), as a function of the gas volume fraction (α). The graphs for C_D vs α are determined with Re =100, except where indicated. The curves of U/U_∞ vs α are valid for $Re \gg 1$ but are not explicitly dependent on Re. The thin solid line represents VPF (expressions 4.2.a and 4.3.a), the thick dashed line represents DM with zero tangential stress on the outer boundary (expressions 4.2.b and 4.3.b), and the thick solid line represents DM with irrotational tangential stress on the outer boundary (expressions 4.2.c and 4.3.c). The thin solid line with open diamond-shaped symbols (◇) represent data from Marrucci,[51] whereas the triangle symbols represent numerical simulations with free-surface cell model by Chhabra[46] for (▲) Re = 20 and (△) and Re =100, where expression 4.6 is used for the normalized velocity. Circular symbols represent numerical simulations with zero-vorticity cell model by Chhabra[46] for (●) Re = 20 and (○) Re =100. DM denotes the dissipation method and VPF denotes viscous potential flow. The symbols for α = 0 correspond to the numerical results by Manjunath et al.,[54] using a free-surface cell model. U_∞ denotes the single bubble rise velocity from the dissipation method.

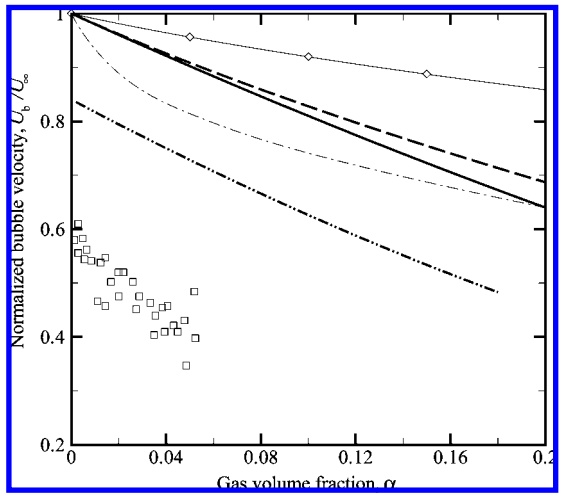

Figure 3. Normalized bubble velocity U_b/U_∞, as a function of the gas volume fraction α, for gas bubbling continuously in a stagnant liquid. Two datasets from experiments are included for comparison. The thick dash-dot-dotted line represents a fitting of data from experiments with nitrogen in aqueous solution (by Zenit et al.[2]); open square symbols (□) represent data from experiments with nitrogen in a water−15 wt % glycerin mixture (by Martinez-Mercado[39]); thick dashed line represents DM with zero tangential stress on the outer boundary (expression 4.3.b); thick solid line represents DM with irrotational tangential stress on the outer boundary (expression 4.3.c); thin dash-dotted line represents the model by Spelt and Sangani[32] (see expression 4.7); and the thin solid line with open diamond-shaped symbols (◇) represent data from Marrucci.[51] "DM" denotes the dissipation method, and "VPF" denotes viscous potential flow. Predictions are given by $U_b = U/(1 - \alpha)$. For the experimental data, U_∞ was determined from Moore's theory.[67]

model gives the lowest normalized velocity among the irrotational theories described in this paper. Slightly higher values are obtained from the DM when a zero tangential stress is prescribed on the outer boundary for the same volume fraction. In addition, results from the former model are somewhat more dependent on the void fraction than results from the latter model. VPF predicts much higher normalized bubble swarm velocities than the other models considered in the analysis, because the first-order viscous correction to the irrotational pressure associated with the vortical layer is omitted, thereby predicting a lower drag. Marrucci's formula predicts dimensionless velocities that lie between those from VPF and the other viscous irrotational theories and shows a less-pronounced dependence on the gas volume fraction.

The results obtained here (plotted as symbols) from the drag coefficients reported in Chhabra[46] from numerical simulations also show a decrease in U/U_∞ as the void fraction α increases. In the limit of infinite dilution, the points included in Figure 2b are given in Manjunath et al.,[54] from their numerical solution. The remark stated above regarding the hindering effect due to increasing gas concentration cannot be drawn from the points determined by the numerical solution, because each data series corresponds to a fixed bubble swarm Reynolds number Re. Because expression 4.6, with the numerical results for C_D in Chhabra,[46] for Re = 20 and 100, yields an increasing Re_∞ as α increases, the ratio Re/Re_∞ and, hence, U/U_∞ should decrease. To investigate the effect of increasing gas volume concentration on bubble rise velocity using numerical simulations at a finite Reynolds number, another type of plot is needed; this can be found elsewhere.[52,53] (See below.) For both Re = 20 and 100 and $\alpha > 0$, the normalized velocity predictions from the free-surface cell model are larger than the results from the zero-vorticity cell model obtained by means of computational fluid dynamics (CFD) analysis. As expected, this trend agrees with that shown by the DM results for U/U_∞ with the zero-tangential-stress model, which leads to somewhat larger values, in comparison with the model with an irrotational tangential stress on the exterior surface. Larger values of U/U_∞ are predicted for bubble swarms with Re = 20 than for swarms with Re = 100 at a fixed gas volume fraction and for the same type of cell model. The difference between both series decreases as the gas volume fraction increases.

The decrease of the normalized bubble swarm velocity U/U_∞ as Re increases for fixed α may be explained by considering the limit of low Reynolds number. For the creeping motion of

a single bubble in an unbounded medium, the drag is known to be $4\pi\mu R_1 U$.[65] Therefore, the bubble terminal rise velocity is $U/U_\infty = 3$, which is well above the corresponding value for $Re = 20$ ($U/U_\infty \approx 1.7$; see Figure 2b). As the Reynolds number increases toward the other limit ($Re \gg 1$), U/U_∞ should tend to 1. This tendency is also observed for a bubble swarm (that is, for $\alpha > 0$).

As the Reynolds number increases, it is reasonable to expect that U/U_∞ for a given value of α approaches the curves resulting from the DM, because these curves represent the limiting values for $Re \gg 1$. Whereas for $\alpha = 0$ and $Re = 100$, $U/U_\infty \approx 1.2$, and a decreasing trend should be expected, so that $U/U_\infty \rightarrow 1$ as Re increases, the data obtained from numerical experiments for $\alpha > 0$ using the free-surface cell model apparently have already reached their limit, given by the DM analysis for the same type of cell model. In the case of the data set corresponding to the zero-vorticity cell model, for $\alpha > 0$, the magnitudes of U/U_∞ are already slightly under their expected limiting values, given by the graph of the DM with an irrotational tangential stress on the exterior boundary. Discarding issues related to the approximations employed in the numerical scheme, one possible explanation for this result is the increasing trend of the product $Re \times C_D$ with increasing Re that, by virtue of expression 4.6, leads to a decrease in U/U_∞. Should this trend be reversed, the product $Re \times C_D$ would start to decrease slowly as Re continues to increase, so that the limiting value would be closely approached, and U/U_∞ would become insensitive to changes in Re.

In closing, one should mention that the results for $U/U_{\alpha=0}$, as a function of the gas volume fraction, with $U_{\alpha=0}$ being the velocity of a bubble rising in an unbounded medium ($U_{\alpha=0} \neq U_\infty$), were reported by LeClair and Hamielec[53] for infinite-dilution Reynolds numbers up to $Re_{\alpha=0} = 1000$ from their numerical solutions, using the zero-vorticity cell model. There, the hindering of bubble motion as the bubble concentration increases is demonstrated from the simulations. They noted that a standing vortex ring in the bubble rear stagnation region was not present. They asserted that, for such a high Reynolds number, the limit given by potential flow theory is approached. From the dissipation method, the drag coefficient defined in expression 4.1 leads to the result $C_D \approx 0.048$, yet they plotted a drag coefficient, defined in the same manner, of $C_D \approx 0.1$. Appreciable covective effects that overcome the capabilities of the numerical scheme[66] are perhaps the cause of such a significant difference. Therefore, we opted not to include their data for such a high Reynolds number in the comparisons made in the present work.

4.2. Comparison of the Theory against Experimental Data. Comparison of the theory with experimental data for the velocity U_b of the bubbles in a bubbly flow, as a function of the void fraction, is presented in Figure 3. One dataset corresponds to the experiments conducted by Zenit et al.[2] to study a monodispersed suspension of bubbles moving in a vertical channel, satisfying the dual limit of large Reynolds numbers and small Weber numbers. The mixture is produced by bubbling gas at a constant volumetric flow rate through a stagnant liquid. They used a dilute aqueous electrolyte solution with nitrogen gas. A monodispersed suspension is obtained with the addition of a salt to the liquid, which helps to prevent bubble coalescence. The mean equivalent bubble diameter of the suspension increases from 1.364 mm to 1.696 mm for gas volume fraction in the interval of $0 \lesssim \alpha \leq 0.20$. The aspect ratio decreases in this interval from 1.3 to 1.1 and the Reynolds and Weber numbers decrease with the void fraction from $Re_b = 380$ and $We_b = 1.5$ for $\alpha \approx 0$ to $Re_b = 260$ and $We_b = 0.5$ for $\alpha = 0.20$. For this data set, Zenit et al.[2] gives the fitting $U_b = U_0(1 - \alpha)^n$, with $U_0 = 0.269$ m/s and $n = 2.796$. They reported that $U_0 < U_\infty = 0.320$ m/s, measured from the rising of a single bubble in a larger pipe; this is a value that is just within 1% of the result predicted by the theory for an oblate ellipsoid.[67] This sudden steep decrease in bubble velocity with gas concentration for very dilute suspensions has been attributed, by Zenit et al.,[2] to the effects of bubble-wall collisions. They discussed this issue in depth while including additional experimental evidence, and the interested reader should refer to their work. Another dataset is taken from the series of experiments performed by Martinez-Mercado et al.[39] with a flux of nitrogen gas bubbling through a variety of stagnant liquids. We choose the set of measurements obtained with a mixture of water and glycerin (15 wt %), because the bubbles were almost spherical and the Reynolds number was $O(100)$. In the experiments with this liquid, the mean bubble diameter decreases from 1.3 mm to 1.2 mm with increasing void fraction from 0 to 0.05, whereas the aspect ratio remained constant ($\sim$1.05). The measured Reynolds and Weber numbers decrease from $Re_b = 120$ and $We_b = 0.60$ to $Re_b = 70$ and $We_b = 0.22$ for void fractions increasing in the range of $0 \lesssim \alpha \leq 0.05$. Again, a rapid decrease in the bubble velocity in the region of a very dilute suspension was observed as the velocity for a single bubble in an infinite medium is 0.287 m/s, computed from the theory for a clean oblate ellipsoidal bubble.[67] (Note that they reported the value of Re_∞ instead.) They speculated that the sudden increase in the drag that slows the bubbles might be caused by velocity fluctuations arising from bubble-wall collisions.

The predictions from the irrotational theories described here are compared with the experimental data for the dimensionless velocity U_b/U_∞ in Figure 3, where U_∞ takes the values given above for both experimental datasets. In addition, Zenit et al.[2] took the model by Spelt and Sangani[32] for the drag coefficient and found an expression for the normalized bubble velocity U_b/U_∞ for vertical bubbly flow through stagnant liquid:

$$\frac{U_b}{U_\infty} = \frac{(1 - \alpha)}{1 + \left(\frac{3}{20}\right)\alpha A} \tag{4.7}$$

Here, parameter A denotes the inverse of the bubble vertical velocity variance normalized by the square of the mean bubble velocity. A fit for $A = A(\alpha)$ with measurements by Zenit et al.[2] is given in the work of Kushch et al.:[30] $A = (0.02 + 0.5\alpha)^{-1}$. This fitting may be regarded as particular for the set of conditions of the experiments from which it is obtained. Predictions from expression 4.7 are included in Figure 3. Note that A does not approach zero as $\alpha \rightarrow 1$; this is explained by the oscillations in the bubble trajectory associated with bubble−wall interactions observed in a single bubble experiment.[2] The drag coefficient formula previously referenced was derived by Spelt and Sangani[32] by solving for a viscous potential that adds a first-order correction in the dimensionless viscosity to the irrotational flow field. Their expression for the drag coefficient was dependent on the void fraction and an additional parameter A (previously defined) and is needed in their system of average equations for bubbly flow in the regime of large Reynolds numbers and small Weber numbers. They presented comparisons with dynamics simulations, in which satisfactory agreement was demonstrated.

The experiments show that a greater concentration of bubbles leads to a hindering of their motion, and the models follow this trend. Figure 3 indicates that the theory overpredicts the measurements in the interval of gas volume fraction considered. This trend has been reported by Zenit et al.[2] from the comparison of their data with the model by Spelt and Sangani.[32] This discrepancy was attributed to several factors, namely, bubble deformation, departures of the liquid dynamics from irrotational motion due to the presence of surface-active contaminants, and energy dissipation associated with bubble shape oscillations.[2] A similar discrepancy was noted by Kushch et al.[30] after comparing their model, derived using an effective-medium theory for oblate spheroidal bubbles, with the data by Zenit et al.[2] They suggested that viscous dissipation that is originated by the container walls might be the cause of such a discrepancy. Figure 3 shows that the model by Spelt and Sangani[32] for U_b/U_∞ presented in Zenit et al.,[2] with the fit for A obtained from their experimental data, gives the least difference with the measurements. Moreover, the difference for all models is the least with the data by Zenit et al.,[2] for which the Reynolds number ($380 \geq Re_b \geq 260$) is ~3 times greater than that of Martinez-Mercado et al.[39] This is consistent with the notion that the formulas considered here are valid for $Re_b \gg 1$, and thus these models should be considered as limiting cases as long as the bubbles remain almost spherical (i.e., $We_b < 1$).

From the set of viscous irrotational theories analyzed in sections 2 and 3 that obtained from the dissipation method with an irrotational tangential stress on the outer boundary gives the smallest discrepancy and also depicts the same slope as the dataset reported by Zenit et al.[2] Nevertheless, when the bubbles are modeled as oblate ellipsoids, using Moore's model for U_∞,[67] and the variation of the equivalent diameter of the bubbles and aspect ratio with the void fraction is taken into account, the curve of U/U_∞ vs α for the experimental data by Zenit et al.[2] becomes rather concave, as presented in their work (not shown here), resembling the curvature of the graph rendered by the model of Spelt and Sangani.[32]

5. Closing Remarks

The assumed irrotational dynamics of the incompressible fluid surrounding a spherical bubble of variable radius and bounded externally by a spherical surface is applied to the computation of the drag acting on the bubble and on the outer surface when a relative translation exists between them. A simpler computation of the drag is given by the integration of the irrotational normal stress, including the viscous part. Another viscous irrotational formulation based on the mechanical energy balance, namely, the dissipation method, is used, leading to a different form of the drag. A major aspect of the formulation of the dissipation method presented here is the way the tangential stress boundary condition on the exterior surface enters the analysis. Two choices are considered for this boundary condition, namely, a zero tangential stress and an irrotational tangential stress. In particular, when the bubble volume is held constant, these expressions for the drag are taken as an approximation, in the sense of the classical cell model, of the drag acting on a swarm of identical bubbles. These results are then used to find expressions for the suitably normalized terminal rise velocity of the bubble swarm. These formulas are evaluated via comparison against other theoretical approaches, numerical simulations of the cell-model, and experimental data for bubbly flow.

The results for the drag coefficient obtained by the dissipation approximation in a cell with either a zero tangential stress or an irrotational tangential stress on the exterior surface show fair agreement with results given in the literature from numerical solutions of the steady incompressible Navier−Stokes equations for a free-surface cell model or a zero-vorticity cell model, respectively, for a bubble-swarm Reynolds number of $Re = 100$. A similar trend is observed for the bubble swarm terminal rise velocity normalized by the terminal rise velocity of a bubble according to the dissipation method, U/U_∞, for nonzero gas volume fraction, $\alpha \geq 0.1$. This bubble swarm rise velocity is found by the equilibration of the viscous drag and bubble weight with the buoyancy force determined by the gas−liquid mixture density. In the infinite dilution limit, the bubble velocity is still larger than the value given by the dissipation method, which should be approached as Re increases. On the other hand, the simpler integration of the normal stress from viscous potential flow gives unsatisfactory predictions. The comparison with the experimental data for bubble velocity in bubbly flow in the regime of high Reynolds numbers and low Weber numbers indicates that the model by Spelt and Sangani,[32] which requires knowledge of the bubble vertical velocity variance, gives the least discrepancy; it is followed by predictions from the dissipation method with an exterior irrotational-tangential-stress boundary condition.

Acknowledgment

We are indebted to Professor R. Fosdick for his contribution in the preparation of Appendix B (this appendix was written by Prof. Fosdick and J.C.P.). This work was partially supported by the National Science Foundation (through Grant No. 0302837). J.C.P. also gratefully acknowledges support from the University of Minnesota Graduate School Dissertation Fellowship. We are thankful to the referees for their constructive criticisms and helpful suggestions that enabled us to improve upon an earlier version of this paper.

Appendix A: Force on the Outer Boundary by the Dissipation Method

In this analysis, we obtain an expression for the force D_2 that the fluid in volume V exerts on the outer boundary S_2 in the $\mathbf{e}_x$-direction using the dissipation method (DM). The analysis involves writing the equations of motion with respect to a noninertial coordinate system. This procedure parallels that of section 2.3 for the force D_1 on the bubble interface S_1 when the outer boundary S_2 is a free surface.

The incompressible Navier−Stokes equations relative to the laboratory reference frame are

$$\rho\left(\frac{\partial \mathbf{u}}{\partial t} + \mathbf{u}\cdot\nabla\mathbf{u}\right) = -\nabla p + \mu\nabla^2\mathbf{u} \tag{A.1}$$

$$\nabla\cdot\mathbf{u} = 0 \tag{A.2}$$

Consider a noninertial reference frame with an origin that moves with velocity $U\mathbf{e}_x$, relative to the laboratory frame, and does not rotate. The transformation between coordinate systems is governed by the relations

$$\hat{\mathbf{x}} = \mathbf{x} - \int_0^t U(t')\mathbf{e}_x\, dt' \tag{A.3.a}$$

$$\hat{t} = t \tag{A.3.b}$$

$$\mathbf{v} = \mathbf{u} - U\mathbf{e}_x \tag{A.3.c}$$

The form of the incompressible Navier−Stokes equations is invariant under the transformation described by expressions A.3.a−A.3.c, provided a pseudo-pressure $\hat{p}$ is defined as[68]

$$\hat{p} \equiv p + \rho \dot{U} \mathbf{e}_x \cdot \hat{\mathbf{x}} \tag{A.4}$$

so that the governing equations in the noninertial reference frame may be written as

$$\rho\left(\frac{\partial \mathbf{v}}{\partial \hat{t}} + \mathbf{v}\cdot\hat{\nabla}\mathbf{v}\right) = -\hat{\nabla}\hat{p} + \mu\hat{\nabla}^2\mathbf{v} \tag{A.5}$$

$$\hat{\nabla}\cdot\mathbf{v} = 0 \tag{A.6}$$

With $\hat{\mathbf{T}} \equiv -\hat{p}\mathbf{1} + \mu(\hat{\nabla}\mathbf{v} + \hat{\nabla}\mathbf{v}^{\mathrm{T}})$, the right-hand side of expression A.5 is $\hat{\nabla}\cdot\hat{\mathbf{T}}$. Moreover, with expression A.4,

$$\hat{\mathbf{T}} = \mathbf{T} - \rho\dot{U}\mathbf{e}_x\cdot\hat{\mathbf{x}} \tag{A.7}$$

Let

$$\hat{D}_2 \equiv \int_{S_2} \mathbf{n}_2\cdot\hat{\mathbf{T}}\cdot\mathbf{e}_x \, dA \tag{A.8}$$

With expressions 2.8 and A.7, expression A.8 yields

$$\hat{D}_2 = D_2 + \int_{S_2} \rho\dot{U}\mathbf{e}_x\cdot\hat{\mathbf{x}}(\mathbf{n}_2\cdot\mathbf{e}_x)\, dA \tag{A.9}$$

The fluid motion is subjected to the following boundary conditions:

On S_1,

$$\mathbf{n}_1\cdot\mathbf{v} = \hat{q}_1 \tag{A.10}$$

$$\mathbf{n}_1\cdot\hat{\mathbf{T}}\cdot\mathbf{t}_1^{(\alpha)} = \mathbf{n}_1\cdot\mathbf{T}\cdot\mathbf{t}_1^{(\alpha)} = 0 \qquad \left(\text{for } \mathbf{t}_1^{(\alpha)}\perp\mathbf{n}_1\right) \tag{A.11}$$

On S_2,

$$\mathbf{n}_2\cdot\mathbf{u} = q_2 \tag{A.12}$$

$$\mathbf{n}_2\cdot\hat{\mathbf{T}}\cdot\mathbf{t}_2^{(\alpha)} = \mathbf{n}_2\cdot\mathbf{T}\cdot\mathbf{t}_2^{(\alpha)} = 0 \qquad \left(\text{for } \mathbf{t}_2^{(\alpha)}\perp\mathbf{n}_2\right) \tag{A.13}$$

and, thus, both surfaces are taken as free surfaces. Taking the inner product of expression A.5 with $\mathbf{v}$ and invoking expression A.6 leads to the mechanical energy equation for the motion relative to the noninertial reference frame. This equation, in integral form, is given as

$$\frac{d\hat{E}}{d\hat{t}} = -\int_{S_1}\mathbf{n}_1\cdot\hat{\mathbf{T}}\cdot\mathbf{v}\, dA + \int_{S_2}\mathbf{n}_2\cdot\hat{\mathbf{T}}\cdot\mathbf{v}\, dA - \int_V 2\mu\hat{\mathbf{D}}[\mathbf{v}]:\hat{\mathbf{D}}[\mathbf{v}]\, dV \tag{A.14}$$

where

$$\frac{d\hat{E}}{d\hat{t}} = \frac{d}{d\hat{t}}\int_V \rho\frac{|\mathbf{v}|^2}{2}\, dV = \int_V \mathbf{v}\cdot\rho\left(\frac{\partial\mathbf{v}}{\partial\hat{t}} + \mathbf{v}\cdot\hat{\nabla}\mathbf{v}\right) dV \tag{A.15}$$

and $\hat{\mathbf{D}}[\mathbf{v}] = {}^1/_2(\hat{\nabla}\mathbf{v} + \hat{\nabla}\mathbf{v}^{\mathrm{T}})$.

With expressions A.3.c, A.8, A.11, and A.13, expression A.14 may be written as

$$\hat{D}_2 = \frac{1}{U}\left(\frac{d\hat{E}}{d\hat{t}} + \int_V 2\mu\hat{\mathbf{D}}[\mathbf{v}]:\hat{\mathbf{D}}[\mathbf{v}]\, dV - \hat{W}\right) \tag{A.16}$$

where

$$\hat{W} = -\int_{S_1}\mathbf{n}_1\cdot\hat{\mathbf{T}}\cdot\mathbf{n}_1\hat{q}_1\, dA + \int_{S_2}\mathbf{n}_2\cdot\hat{\mathbf{T}}\cdot\mathbf{n}_2 q_2\, dA \tag{A.17}$$

Now, the integrals in the left-hand side of expression A.16 are evaluated in potential flow, $\mathbf{v} = \hat{\nabla}\hat{\phi}$. The momentum balance (expression A.5) reduces to the Bernoulli equation for potential flow, i.e.,

$$\frac{\hat{p}}{\rho} + \frac{\partial\hat{\phi}}{\partial\hat{t}} + \frac{|\mathbf{v}|^2}{2} = B(\hat{t}) \tag{A.18}$$

Then, expression A.15 yields

$$\frac{d\hat{E}}{d\hat{t}} = -\int_{S_1}(-\hat{p})\hat{q}_1\, dS + \int_{S_2}(-\hat{p})\hat{q}_2\, dS - U\int_{S_2}(-\hat{p})\mathbf{n}_2\cdot\mathbf{e}_x\, dS \tag{A.19}$$

Denoting $\hat{\mathbf{D}} = \hat{\mathbf{D}}[\mathbf{v} = \nabla\hat{\phi}]$, the dissipation integral in expression A.16 becomes

$$\begin{aligned}\int_V 2\mu\hat{\mathbf{D}}:\hat{\mathbf{D}}\, dV &= -\int_{S_1}\mathbf{n}_1\cdot 2\mu\hat{\mathbf{D}}\cdot\mathbf{v}\, dA + \int_{S_2}\mathbf{n}_2\cdot 2\mu\hat{\mathbf{D}}\cdot\mathbf{v}\, dA \\ &= -\int_{S_1}\mathbf{n}_1\cdot 2\mu\hat{\mathbf{D}}\cdot\mathbf{n}_1\hat{q}_1\, dA - \int_{S_1}\mathbf{n}_1\cdot 2\mu\hat{\mathbf{D}}\cdot\mathbf{t}_1^{(\alpha)}(\mathbf{t}_1^{(\alpha)}\cdot\mathbf{v})\, dA - \\ &\quad U\int_{S_2}\mathbf{n}_2\cdot 2\mu\hat{\mathbf{D}}\cdot\mathbf{e}_x\, dA + \int_{S_2}\mathbf{n}_2\cdot 2\mu\hat{\mathbf{D}}\cdot\mathbf{n}_2 q_2\, dA + \\ &\quad \int_{S_2}\mathbf{n}_2\cdot 2\mu\hat{\mathbf{D}}\cdot\mathbf{t}_2^{(\alpha)}(\mathbf{t}_2^{(\alpha)}\cdot\mathbf{u})\, dA\end{aligned} \tag{A.20}$$

using the relation $\mathbf{v} = \mathbf{u} - U\mathbf{e}_x$ and boundary conditions described by expressions A.10 and A.12. Substitution of expressions A.19 and A.20 into expression A.16, with expression A.17 given by potential flow, leads to

$$\begin{aligned}\hat{D}_2 = &-\int_{S_2}(-\hat{p} + \mathbf{n}_1\cdot 2\mu\hat{\mathbf{D}}\cdot\mathbf{n}_2)\mathbf{n}_2\cdot\mathbf{e}_x\, dA + \\ &\frac{1}{U}\int_{S_2}\mathbf{n}_2\cdot 2\mu\hat{\mathbf{D}}\cdot\mathbf{t}_2^{(\alpha)}(\mathbf{t}_2^{(\alpha)}\cdot\mathbf{v})\, dA \\ &-\frac{1}{U}\int_{S_1}\mathbf{n}_1\cdot 2\mu\hat{\mathbf{D}}\cdot\mathbf{t}_1^{(\alpha)}(\mathbf{t}_1^{(\alpha)}\cdot\mathbf{v})\, dA\end{aligned} \tag{A.21}$$

Using expressions A.4 and A.9, with $\mathbf{D} = \mathbf{D}[\mathbf{u}] = \hat{\mathbf{D}}[\mathbf{v}]$ from the transformation described by expression A.3, expression A.21 results in expression 2.34 that is given in section 2.3.1.

Finally, expression 2.35 for $D_1 + D_2$ is obtained using the self-equilibration of irrotational viscous stresses. This implies

$$\int_V \nabla\cdot 2\mu\mathbf{D}\cdot\mathbf{e}_x\, dV = -\int_{S_1}\mathbf{n}_1\cdot 2\mu\mathbf{D}\cdot\mathbf{e}_x\, dA - \int_{S_2}\mathbf{n}_2\cdot 2\mu\mathbf{D}\cdot\mathbf{e}_x\, dA = 0 \tag{A.22}$$

which results in the relation

$$\begin{aligned}&\int_{S_1}\mathbf{n}_1\cdot 2\mu\mathbf{D}\cdot\mathbf{n}_1(\mathbf{n}_1\cdot\mathbf{e}_x)\, dA + \int_{S_1}\mathbf{n}_1\cdot 2\mu\mathbf{D}\cdot\mathbf{t}_1^{(\alpha)}(\mathbf{t}_1^{(\alpha)}\cdot\mathbf{e}_x)\, dA \\ &= \int_{S_2}\mathbf{n}_2\cdot 2\mu\mathbf{D}\cdot\mathbf{n}_2(\mathbf{n}_2\cdot\mathbf{e}_x)\, dA + \int_{S_2}\mathbf{n}_2\cdot 2\mu\mathbf{D}\cdot\mathbf{t}_2^{(\alpha)}(\mathbf{t}_2^{(\alpha)}\cdot\mathbf{e}_x)\, dA = 0\end{aligned} \tag{A.23}$$

The reason why *each* of the surface integrals in expression A.22 vanishes is shown in Appendix B.

Appendix B: The Net Resultant of the Viscous Stress on a Closed Surface in Potential Flow

Consider a closed surface S bounding a region V of incompressible Newtonian fluid in which the motion is irrotational. The deviatoric stress is given by $\tau = 2\mu\nabla\otimes\nabla\phi$, where ϕ is the velocity potential that satisfies the Laplace's equation in V, by continuity, and μ is the dynamic viscosity. Then, the divergence of τ is zero in V. As a consequence, the statement "the traction vectors $\mathbf{n}\cdot\boldsymbol{\tau}$ have no net resultant on each and every closed surface in the domain V of flow"[69] follows immediately, because

$$\int_D \nabla\cdot\boldsymbol{\tau}\, dV = \int_\Gamma \mathbf{n}\cdot\boldsymbol{\tau}\, dA = 0 \tag{B.1}$$

using the divergence theorem, where D is an arbitrary volume in V with boundary Γ, and $\mathbf{n}$ is the outward normal unit vector

to Γ. The surface integral in expression B.1 represents the net irrotational viscous stress over Γ.

A proof of the above statement that the surface integral in expression B.1 vanishes for every closed surface in the fluid domain is not obvious for a "periphractic" region. A three-dimensional region is periphractic "when it is bounded internally by one or more closed surfaces" (from Milne-Thomson,[70] p 97). Thus, a periphractic region has one or more holes embedded in it, but no hole runs through the outer boundary, and, thus, the volume is simply connected.

Consider now a periphractic three-dimensional region bounded externally by a surface S enclosing a fluid volume V and one or more embedded holes. Suppose the fluid motion in V is irrotational. Consider a closed surface Γ immersed in V. This surface may surround a volume totally filled with fluid or there can be one or more holes enclosed by Γ. We wish to show that

$$\int_\Gamma \mathbf{n}\cdot\boldsymbol{\tau}\,\mathrm{d}A = \int_\Gamma \mathbf{n}\cdot 2\mu\nabla\otimes\nabla\phi\,\mathrm{d}A = 0 \tag{B.2}$$

Using Cartesian index notation, given that $\tau_{ij} = 2\mu\phi_{,ij}$ and $\phi_{,ii} = 0$, where the comma in the subscript denotes partial differentiation with respect to the Cartesian coordinates indexed after it, we may write

$$\tau_{ij} = \varepsilon_{ikl}\varepsilon_{jrs}B_{rk,st} \tag{B.3}$$

provided we use

$$B_{rk} \equiv -2\mu\delta_{rk}\phi \tag{B.4}$$

where ε_{ijk} is the permutation symbol and δ_{ij} is the Kronecker delta. This follows by a simple reduction of indices, because, with expression B.4, expression B.3 yields

$$\begin{aligned}\tau_{ij} &= -2\mu\varepsilon_{ikl}\varepsilon_{jrs}\delta_{rk}\phi_{,st} = -2\mu\varepsilon_{ikl}\varepsilon_{jks}\phi_{,st}\\ &= -2\mu(\delta_{ts}\delta_{ij} - \delta_{tj}\delta_{is})\phi_{,st} = 2\mu\phi_{,ij}\end{aligned} \tag{B.5}$$

The form of expression B.3 is known as a "Beltrami representation" of the stress (see section 4 in the work of Fosdick and Royer-Carfagni[71]). Note that τ_{ij} is symmetric, provided that B_{ij} is also symmetric. Now, with this representation and using Stokes' theorem, we have

$$\int_\Gamma n_i\Gamma_{ij}\,\mathrm{d}A = \int_\Gamma n_i\varepsilon_{ikl}\varepsilon_{jrs}B_{rk,st}\,\mathrm{d}A = 0 \tag{B.6}$$

for every closed surface Γ in V. Thus, expression B.2 holds and the net viscous irrotational stress on any closed surface Γ in V is zero.

It is also true that, because of the aforementioned Beltrami representation, the moment of the irrotational viscous stress on every closed surface Γ in V about any fixed point (for example, the origin of the coordinate system) is zero. That is,

$$\int_\Gamma \mathbf{x}\times(n\cdot\boldsymbol{\tau})\,\mathrm{d}A = 0 \tag{B.7}$$

or, in Cartesian index notation,

$$\int_\Gamma \varepsilon_{lmj}\mathbf{x}_m n_i\boldsymbol{\tau}_{ij}\,\mathrm{d}A = 0 \tag{B.8}$$

By applying the divergence theorem, Joseph[72] obtained expression B.7 without using the representation described by expression B.3 for a region with no embedded holes.

Both balances together indicate that any closed surface Γ in V is "self-equilibrated". Results from expressions B.2 and B.7 apply, in particular, to the outer and inner boundaries of V.

Appendix C: Velocity Potential Coefficients

The expression for q_1 in expression 3.5 may be rewritten in terms of Legendre polynomials as

$$q_1 = \dot{R}_1 + \dot{\epsilon}P_1(z) - \frac{2}{3}\frac{\epsilon\dot{\epsilon}}{R_1}(1 - P_2(z)) + O(\epsilon^2) \tag{C.1}$$

where $z = \cos\theta$. Using expression 3.4 for the potential ϕ, expression 3.10 for coefficients A_l and B_l, and expression 3.7 for $\mathbf{n}_1$, we can compute

$$\begin{aligned}\mathbf{n}_1\cdot\nabla\phi\Big|_{s_1} &= -B_0R_1^{-2} + 2\epsilon B_0R_1^{-3}P_1(z) +\\ &\sum_{l=1}^{\infty}[lA_l^{(0)}R_1^{l-1} - (l+1)B_l^{(0)}R_1^{-l-2}]P_l(z) +\\ &\epsilon\sum_{l=1}^{\infty}[lA_l^{(1)}R_1^{l-1} - (l+1)B_l^{(1)}R_1^{-l-2}]P_l(z) +\\ &\epsilon\sum_{l=2}^{\infty}[(l-1)^2A_{l-1}^{(0)}R_1^{l-3} + \{(l+1)^2 - 2\}\times\\ &B_{l-1}^{(0)}R_1^{-l-2}]\frac{l}{2l-1}P_l(z) + \epsilon\sum_{l=0}^{\infty}[(l^2-2)A_{l+1}^{(0)}R_1^{l-1} +\\ &(l+2)^2B_{l+1}^{(0)}R_1^{-l-4}]\frac{l+1}{2l+3}P_l(z) + O(\epsilon^2)\end{aligned} \tag{C.2}$$

Then, satisfying expression 3.5 with expressions C.1 and C.2, applying orthogonality of Legendre polynomials, and equating terms of alike powers of ϵ, results in this set of relations for the coefficients in expression 3.10:

$$-B_0R_1^{-2} = \dot{R}_1 \tag{C.3}$$

$$A_1^{(0)} - 2B_1^{(0)}R_1^{-3} = \dot{\epsilon} \tag{C.4}$$

$$2B_0R_1^{-3} + A_1^{(1)} - 2B_1^{(1)}R_1^{-3} + \frac{2}{5} - (A_2^{(0)} + 9B_2^{(0)}R_1^{-5}) = 0 \tag{C.5}$$

$$2A_2^{(0)}R_1 - 3B_2^{(0)}R_1^{-4} = 0 \tag{C.6}$$

$$\begin{aligned}&2A_2^{(1)}R_1 - 3B_1^{(2)}R_1^{-4} + \frac{2}{3}(A_1^{(0)}R_1^{-1} + 7B_2^{(0)}R_1^{-4}) +\\ &\frac{3}{7}(2A_3^{(0)}R_1 + 16B_3^{(0)}R_1^{-6}) = \frac{2}{3}\left(\frac{\dot{\epsilon}}{R_1}\right)\end{aligned} \tag{C.7}$$

and, for $l \geq 3$,

$$lA_l^{(0)}R_1^{l-1} - (l+1)B_l^{(0)}R_1^{-l-2} = 0 \tag{C.8}$$

$$\begin{aligned}&lA_l^{(1)}R_1^{l-1} - (l+1)B_l^{(1)}R_1^{-l-2} + [(l-1)^2A_{l-1}^{(0)}R_1^{l-3} +\\ &\{(l+1)^2 - 2\}B_{l-1}^{(0)}R_1^{-l-2}]\frac{l}{2l-1} + [(l^2-2)A_{l+1}^{(0)}R_1^{l-1} +\\ &(l+2)^2B_{l+1}^{(0)}R_1^{-l-4}]\frac{l+1}{2l+3} = 0\end{aligned} \tag{C.9}$$

Furthermore, we recall expressions 3.8 and 3.9,

$$B_0 = -R_2^2\dot{R}_2 = -R_1^2\dot{R}_1 \tag{3.8}$$

$$A_lR_2^{l-1} = B_l(l+1)R_2^{-l-2} \qquad (\text{for } l \geq 1) \tag{3.9}$$

respectively. Note that expression C.3 is satisfied by expression 3.8.

From expressions C.6 and C.8, using expression 3.9, we obtain $A_l^{(0)} = B_l^{(0)} = 0$ for $l \geq 2$. Then, using these results in expression C.9, in combination with expression 3.9, yields $A_l^{(1)} = B_l^{(1)} = 0$ for $l \geq 3$.

Next, the system that is defined by expressions C.4−C.7 yields expressions for $A_1^{(0)}$, $B_1^{(0)}$, $A_1^{(1)}$, and $B_1^{(1)}$. This leads to expression 3.11, in addition to $A_2^{(1)}$ and $B_2^{(1)}$, after some algebra. That is, to first order in ϵ,

$$A_2 = -\frac{3\epsilon\dot{\epsilon}R_1^{\,3}R_2^{\,3}}{2(R_2^{\,3} - R_1^{\,3})(R_2^{\,5} - R_1^{\,5})},$$

$$B_2 = -\frac{\epsilon\dot{\epsilon}R_1^{\,3}R_2^{\,8}}{(R_2^{\,3} - R_1^{\,3})(R_2^{\,5} - R_1^{\,5})} \quad \text{(C.10)}$$

Notice that, although $A_2 = B_2 = 0$ for $\epsilon = 0$, their time derivatives, which are needed in the unsteady Bernoulli equation, generally do not vanish at $\epsilon = 0$. However, it turns out that the $l = 2$ terms do not contribute at all to the forces on S_1 and S_2 in the $\mathbf{e}_x$-direction with $\epsilon = 0$, because of the orthogonality of Legendre polynomials.

Literature Cited

(1) Levich, V. G. *Physicochemical Hydrodynamics*; Prentice−Hall: Englewood Cliffs, NJ, 1962; Sections 80−83.

(2) Zenit, R.; Koch, D. L.; Sangani, A. Measurements of the Average Properties of a Suspension of Bubbles Rising in a Vertical Channel. *J. Fluid Mech.* **2001**, *429*, 307.

(3) Sangani, A. S.; Didwania, A. K. Dynamic Simulations of Flow of Bubbly Liquids at Large Reynolds Numbers. *J. Fluid Mech.* **1993**, *250*, 307.

(4) Kang, S.-Y.; Sangani, A. S.; Tsao, H.-K.; Koch, D. L. Rheology of dense bubble suspensions. *Phys. Fluids* **1997**, *9*, 1540.

(5) Sankaranarayanan, K.; Shan, X.; Kevrekidis, I. G.; Sundaresan, S. Analysis of Drag and Virtual Mass Forces in Bubbly Suspensions Using an Implicit Formulation of the Lattice Boltzmann Method. *J. Fluid Mech.* **2002**, *452*, 61.

(6) Esmaeeli, A.; Tryggvason, G. A Direct Numerical Simulation Study of the Buoyant Rise of Bubbles at *O*(100) Reynolds Number. *Phys. Fluids* **2005**, *17*, 093303.

(7) Landau, L. D.; Lifshitz, E. M. *Fluid Mechanics*; Course of Theoretical Physics, Vol. 6; Pergamon Press: Oxford, U.K., 1959; Section 25.

(8) Dryden, H.; Murnaghan, F.; Bateman, H. *Hydrodynamics*; Dover: New York, 1956; Part II, Section 1.1. (A complete unabridged reprinting of the National Research Council's Bulletin 84, 1931.)

(9) Ackeret, J. Über exakte Lösungen der Stokes-Navier-Gleichungen inkompressibler Flüssigkeiten bei veränderten Grenzbedingungen. *Z. Angew. Math. Phys.* **1952**, *3*, 259.

(10) Levich, V. G. The Motion of Bubbles at High Reynolds Numbers. *Zh. Eksp. Teor. Fiz.* **1949**, *19*, 18.

(11) Joseph, D. D.; Liao, T. Y. Potential Flows of Viscous and Viscoelastic Fluids. *J. Fluid Mech.* **1994**, *265*, 1.

(12) Moore, D. W. The Boundary Layer on a Spherical Gas Bubble. *J. Fluid. Mech.* **1963**, *16*, 161.

(13) Kang, I. S.; Leal, L. G. The Drag Coefficient for a Spherical Bubble in a Uniform Streaming Flow. *Phys. Fluids* **1988**, *31*, 233.

(14) Joseph, D. D.; Wang, J. The Dissipation Approximation and Viscous Potential Flow. *J. Fluid Mech.* **2004**, *505*, 365.

(15) Moore, D. W. The Rise of a Gas Bubble in a Viscous Liquid. *J. Fluid. Mech.* **1959**, *6*, 113.

(16) Tam, P. D. The Unsteady Drag on a Spherical Bubble at Large Reynolds Numbers. *Appl. Sci. Res.* **1982**, *38*, 247.

(17) Miksis, M.; Vanden-Broeck, J.-M.; Keller, J. B. Rising Bubbles. *J. Fluid. Mech.* **1982**, *123*, 31.

(18) Magnaudet, J.; Legendre, D. The Viscous Drag Force on a Spherical Bubble with a Time-Dependent Radius. *Phys. Fluids* **1998**, *10*, 550.

(19) Ohl, C. D.; Tijink, A.; Prosperetti, A. The Added Mass of an Expanding Bubble. *J. Fluid Mech.* **2003**, *482*, 271.

(20) Yang, B.; Prosperetti, A.; Takagi, S. The Transient Rise of a Bubble Subject to Shape or Volume Changes. *Phys. Fluids* **2003**, *15*, 2640.

(21) Takemura, F.; Magnaudet, J. The History Force on a Rapidly Shrinking Bubble Rising at Finite Reynolds Number. *Phys. Fluids* **2004**, *16*, 3247.

(22) Léger, D.; Askovic, R. Viscid Contributions to the Hydrodynamic Flows Past a Rising Spherical Gas Bubble with a Time-Dependent Radius. *Int. J. Non-Linear Mech.* **2006**, *41*, 247.

(23) Magnaudet, J.; Eames, I. The Motion of High-Reynolds-Number Bubbles in Inhomogeneous Flows. *Annu. Rev. Fluid Mech.* **2000**, *32*, 659.

(24) Kulkarni, A.; Joshi, J. Bubble Formation and Bubble Rise Velocity in Gas-Liquid Systems: A Review. *Ind. Eng. Chem. Res.* **2005**, *44*, 5873.

(25) Voinov, O. V; Golovin, A. M. Lagrange Equations for a System of Bubbles of Varying Radii in a Liquid of Small Viscosity. *Fluid Dyn.* **1970**, *5*, 458.

(26) Gavrilyuk, S. L.; Teshukov, V. M. Drag Force Acting on a Bubble in a Cloud of Compressible Spherical Bubbles at Large Reynolds Numbers. *Eur. J. Mech. B: Fluids* **2005**, *24*, 468.

(27) Ilinskii, Y.; Hamilton, M. F.; Zabolotskaya, E. A. Bubble Interaction Dynamics in Lagrangian and Hamiltonian Mechanics. *J. Acoustic Soc. Am.* **2007**, *121*, 786.

(28) Smereka, P. On the Motion of Bubbles in a Periodic Box. *J. Fluid Mech.* **1993**, *254*, 79.

(29) Wang, N.; Smereka, P. Effective Equations for Sound and Void Wave Propagation in Bubbly Fluids. *SIAM J. Appl. Math.* **2003**, *63*, 1849.

(30) Kushch, V.; Sangani, A. S.; Spelt, P. D. M.; Koch, D. Finite-Weber-Number Motion of Bubbles through a Nearly Inviscid Liquid. *J. Fluid Mech.* **2002**, *460*, 241.

(31) Sangani, A. S. A Pairwise Interaction Theory for Determining the Linear Acoustic Properties of Dilute Bubbly Liquids. *J. Fluid Mech.* **1991**, *232*, 221.

(32) Spelt, P. D. M.; Sangani, A. S. Properties and Average Equations for Flows of Bubbly Liquids. *Appl. Sci. Res.* **1998**, *58*, 337.

(33) Zhang, D. Z.; Prosperetti, A. Ensemble Phase-Averaged Equations for Bubbly Flows. *Phys. Fluids* **1994**, *6*, 2956.

(34) Esmaeeli, A.; Tryggvason, G. Direct Numerical Simulations of Bubbly Flows. Part I−Low Reynolds Number Arrays. *J. Fluid Mech.* **1998**, *377*, 313.

(35) Esmaeeli, A.; Tryggvason, G. Direct Numerical Simulations of Bubbly Flows. Part II−Moderate Reynolds Number Arrays. *J. Fluid Mech.* **1999**, *385*, 325.

(36) Bunner, B.; Tryggvason, G. Dynamics of Homogeneous Bubbly Flows. Part 1. Rise Velocity and Microstructure of the Bubbles. *J. Fluid Mech.* **2002**, *466*, 17.

(37) Bunner, B.; Tryggvason, G. Dynamics of Homogeneous Bubbly Flows. Part 2. Velocity Fluctuations. *J. Fluid Mech.* **2002**, *466*, 53.

(38) Yin, X.; Koch, D.; Verberg, R. Lattice−Boltzmann Method for Simulating Spherical Bubbles with No Tangential Stress Boundary Conditions. *Phys. Rev. E* **2006**, *73*, 026301.

(39) Martinez-Mercado, J.; Palacios-Morales, C. A.; Zenit, R. Measurement of Pseudoturbulence Intensity in Monodispersed Bubbly Liquids for $10 < Re < 500$. *Phys. Fluids* **2007**, *19*, 103302.

(40) Spelt, P. D. M.; Norato, M. A.; Sangani, A. S.; Greenwood, M. S.; Tavlarides, L. Attenuation of Sound in Concentrated Suspensions: Theory and Experiments. *J. Fluid Mech.* **2001**, *430*, 51.

(41) Dodd, T. L.; Hammer, D. A.; Sangani, A. S.; Koch, D. L. Numerical Simulations of the Effect of Hydrodynamic Interactions on Diffusivities of Integral Membrane Proteins. *J. Fluid Mech.* **1995**, *293*, 147.

(42) Sangani, A. S.; Mo, G. Elastic Interactions in Particulate Composites with Perfect as well as Imperfect Interfaces. *J. Mech. Phys. Solids* **1997**, *45*, 2001.

(43) Koo, S.; Sangani, A. S. Effective-Medium Theories for Predicting Hydrodynamics Transport Properties of Bidisperse Suspensions. *Phys. Fluids* **2002**, *14*, 3522.

(44) Koo, S.; Sangani, A. S. Mass Transfer Coefficients for Laminar Longitudinal Flow in Hollow-Fibre Contactors. *J. Fluid Mech.* **2003**, *484*, 255.

(45) Happel, J.; Brenner, H. *Low Reynolds Number Hydrodynamics*; Prentice−Hall: Englewood Cliffs, NJ, 1965; Section 8.4.

(46) Chhabra, R. P. Further Remarks on the Drag of a Swarm of Bubbles. *Int. J. Eng. Sci.* **1995**, *33*, 1849.

(47) Cunningham, E. On the Velocity of Steady Fall of Spherical Particles Through Fluid Medium. *Proc. R. Soc. London A* **1910**, *A83*, 357.

(48) Happel, J. Viscous Flow in Multiparticle Systems: Slow Motion of Fluids Relative to Beds of Spherical Particles. *AIChE J.* **1958**, *4*, 197.

(49) Kuwabara, S. The Forces Experienced by Randomly Distributed Parallel Circular Cylinders or Spheres in a Viscous Flow at Small Reynolds Numbers. *J. Phys. Soc. Jpn.* **1959**, *14*, 527.

(50) El-Kaissy, M. M.; Homsy, G. M. A Theoretical Study of Pressure Drop and Transport in Packed Beds at Intermediate Reynolds Numbers. *Ind. Eng. Chem. Fundam.* **1973**, *12*, 82.

(51) Marrucci, G. Rising velocity of a Swarm of Spherical Bubbles. *Ind. Eng. Chem. Fundam.* **1965**, *5*, 224.

(52) Kendoush, A. A. Hydrodynamic Model for Bubbles in a Swarm. *Chem. Eng. Sci.* **2001**, *56*, 235.

(53) LeClair, B. P.; Hamielec, A. E. Viscous Flow through Particle Assemblages at Intermediate Reynolds Numbers−A Cell Model for Transport in Bubble Swarms. *Can. J. Chem. Eng.* **1971**, *49*, 713.

(54) Manjunath, M.; Tripathi, A.; Chhabra, R. P.; Sundararajan, T. Numerical Simulation of the Drag on a Swarm of Bubbles. *Int. J. Eng. Sci.* **1994**, *32*, 927.

(55) Sherwood, J. D. The Force on a Growing Bubble in Potential Flow. *Int. J. Multiphase Flow* **1999**, *25*, 705.

(56) Joseph, D. D.; Liao, T. Y.; Hu, H. H. Drag and Moment in Viscous Potential Flow. *Eur. J. Mech. B: Fluids* **1993**, *12*, 97.

(57) Strauss, W. A. *Partial Differential Equations: An Introduction*; John Wiley & Sons: Hoboken, NJ, 1992; Section 10.6.

(58) Zuber, N. On the Dispersed Two-Phase Flow in the Laminar Flow Regime. *Chem. Eng. Sci.* **1964**, *19*, 897.

(59) Joseph, D. D.; Funada, T.; Wang, J. *Potential Flow of Viscous and Viscoelastic Fluids*; Cambridge University Press: New York, 2007; Section 12.5.

(60) Nicklin, D. J. Two-phase bubble flow. *Chem. Eng. Sci.* **1962**, *17*, 693.

(61) Zuber, N.; Hench, J. Steady State and Transient Void Fraction of Bubbling Systems and their Operating Limits, Part 1: Steady State Operation. Report No. 62GL100, General Electric Company, General Engineering Laboratory, New York, 1962.

(62) Richardson, J. F.; Zaki, W. N. Sedimentation and Fluidisation: Part I. *Trans. Inst. Chem. Eng.* **1954**, *32*, 35.

(63) Poletto, M.; Joseph, D. D. Effective Density and Viscosity of a Suspension. *J. Rheol.* **1995**, *39*, 323.

(64) Ishii, M.; Zuber, N. Drag Coefficient and Relative Velocity in Bubbly, Droplet or Particulate Flows. *AIChE J.* **1979**, *25*, 843.

(65) White, F. M. *Viscous Fluid Flow*; McGraw−Hill: New York, 1974; Section 3.10.

(66) Jaiswal, A. K.; Sundararajan, T.; Chhabra, R. P. Simulation of Non-Newtonian Fluid Flow through Fixed and Fluidized Beds of Spherical Particles. *Numer. Heat Transfer, Part A* **1992**, *21*, 275.

(67) Moore, D. W. The Velocity of Rise of Distorted Gas Bubbles in a Liquid of Small Viscosity. *J. Fluid Mech.* **1965**, *23*, 749.

(68) Panton, R. L. *Incompressible Flow*, Third Edition; Wiley: Hoboken, NJ, 2005; Section 10.7.

(69) Joseph, D. D. Helmholtz Decomposition Coupling Rotational to Irrotational Flow of a Viscous Fluid. *Proc. Natl. Acad. Sci., U.S.A.* **2006**, *103*, 14272.

(70) Milne-Thomson, L. M. *Theoretical Hydrodynamics*, Fifth Edition; Macmillan: London, 1968, Section 3.75. (Unabridged republication by Dover, New York, 1996.)

(71) Fosdick, R.; Royer-Carfagni, G. A Stokes Theorem for Second Order Tensor Fields and Its Implications in Continuum Mechanics. *Int. J. Non-Linear Mech.* **2005**, *40*, 381.

(72) Joseph, D. D. The Role of Potential Flow in the Theory of the Navier−Stokes Equations. In *Advances in Mathematical Fluid Mechanics* (Dedicated to Giovanni Paolo Galdi on the occasion of His 60th Birthday); Rannacher, R., sequeira, A., Eds.; Springer: New York, 2008.

Received for review February 12, 2008
Revised manuscript received July 25, 2008
Accepted July 28, 2008

IE800251J